February 9, 2022

Dear editor,

Thank you for providing us the opportunity to revise and improve our manuscript entitled "Measurement report: The importance of biomass burning in light extinction and direct radiative effect of urban aerosol during the COVID-19 lockdown in China" by Tian et al. We are also grateful for the valuable comments and suggestions raised by reviewers.

We have made the changes suggested by reviewers and have outlined those changes in detail below. The modifications can be tracked in the revised manuscript.

Sincerely yours,

Qiyuan Wang
Institute of Earth Environment, Chinese Academy of Sciences
Address: 97 Yanxiang Road, Yanta District, Xi'an 710061, China.
E-mails: wangqy@ieecas.cn
Tel: +86-29-62336205
Fax: +86-29-62336234

Responses to Referee #1:

General comments:

Urbanization even anthropogenic activities is an important way to influence air pollution by emissions (gases and particles), meteorological conditions and atmospheric processes (urban heat island), etc. Anthropogenic pollutants include greenhouse gases, gaseous and particulate pollutants. Aerosol is very important to impact atmospheric cycle and climate system by direct and indirect effects, a hot issue of scientific researches internationally. Also, atmospheric pollutions cause adverse harm to human health. Aerosols are known to originate from direct emission and secondary formation, namely, POA and SOA. The organic aerosol (OA) is a very important part of aerosols, including BC and OC. Inorganic ions are important compositions of aerosols. This paper used the data of aerosol optical properties, chemical composition, meteorological parameters used in Xi'an to analyze their temporal variation and compare their difference between the normal period and the COVID-19 in 2019, and to estimate the radiation forcing of aerosols. The topic of this paper is of common interest within the scientific community. Although the manuscript includes some important data, however, the quality is somewhat sufficient in the current state to be directly published.

Response: We thank the reviewer for the careful evaluation of our manuscript. We have revised the manuscript and provided more elaborations on the datasets according to both reviewers. Besides, the language has been also polished by a native English speaker. We believe that the quality of the revised manuscript has been greatly improved.

Responses to Referee #2:

General comments:

This work analyzes the impact of the COVID-19 lockdown in China on some atmospheric properties, in particular on the extinction, scattering and absorbing coefficients together with the direct radiative effect, all of them considering the aerosol chemical composition. The topic is clearly in the scope of Atmospheric Chemistry and Physics, and absolutely relevant for the scientific community and decision-makers. The manuscript is very well written, with only few typos. My main concerns (general comments) are three:

Response: We appreciate the thoughtful and valuable suggestions by the reviewer, which are helpful for us to improve the quality of our manuscript. We have addressed the comments in point-by-point form as shown below.

Comment (1): Title does not reflect the actual content of the work. The current title is quite ambiguous, leading the reader to expect a study on the entire Chinese territory. I suggest to explicit that the analysis focuses on the study case in Xi'an.

Response: Suggestion taken. The title has been revised to "Measurement report: The importance of biomass burning in light extinction and direct radiative effect of urban aerosol during the COVID-19 lockdown in Xi'an, China".

Comment (2): the sampling campaign consisted of two distinct periods, the so-called normal period (1 to 23 January, 2020) and COVID-19 lockdown period (27 January to 7 February, 2020). Because the aim of the study is to compare the atmosphere during lockdown period against the 'normal' conditions, I consider the normal period chosen here inappropriate. Would it not be more correct to compare with the historical period 27 January 7 February (i.e. average of several years to minimize the effect of different meteorological conditions)?

Response: Thank you for pointing this out. We do agree that a comparison between the COVID-19 lockdown period and the historical same period could minimize the uncertainty of the effects of meteorological conditions. Our intensive online measurement was performed from January 1st to February 9th, 2020. Unfortunately, after consulting the local researchers and authorizations and full literature searching on the databases, there was no matching data availability during the same period before 2020. In this study, the generalized additive model analysis that was described in Section 3.2 indicated the reduction of aerosol light extinction from normal period to lockdown period was credited to anthropogenic emission reduction. The normal period of January 1st to 23rd, 2020 that did not disturb by any special event and was the closest time theme acted as a reasonable and appropriate reference period to investigate the impacts of anthropogenic emission on the optical property and direct radiative effect of aerosol during the lockdown period.

Comment (3): there are a lot of figures as supplementary material. Please considered to move some of them to the main manuscript. I suggest to include figures S8, S9 and S13.

Response: Following the reviewer's suggestion, Figures S8 and S9 have been moved to the main manuscript and assigned as Figures 1 and 2, respectively. Figure S13 shows the realistic AAE of BC during the normal and lockdown periods, which was used for the calculation with the Absorption Ångström exponent method (see details in Text S1 as supplementary material). Therefore, we believe that Figure S13 is more appropriate to be kept in the supplementary material as well.

Specific comments:
Comment (4): Line 15: replace 'optical properties of aerosol' by 'aerosol optical properties'.

Response: The phrase "optical properties of aerosol" has been replaced by "aerosol optical properties".

Comment (5): Lines 39-40: Specify that this sentence refers only to China or include other references with studies worldwide (e.g. Ibrahim et al., 2021). Ibrahim, S., Landa, M., Pešek, O., Pavelka, K., & Halounova, L. (2021). Space-Time Machine Learning Models to Analyze COVID-19 Pandemic Lockdown Effects on Aerosol Optical Depth over Europe. Remote Sensing, 13(15), 3027.

Response: In the revised manuscript, more important worldwide references have been added (e.g., Ibrahim et al., 2021; Kumar et al., 2021; Sanap, 2021; Weber et al., 2020). Besides, our original phrase "recent aerosol studies" refers to China only. The relevant description has been revised as follows:

Page 2 Line 34–44: "The abrupt outbreak of Coronavirus Disease 2019 (COVID-19) caused unprecedented economic and social disruption (Yao et al., 2020). Most worldwide countries implemented the city lockdown to curb the virus spread among humans, providing a rare opportunity to investigate the impacts of anthropogenic activities on the air quality (Ibrahim et al., 2021; Kumar et al., 2021; Sanap, 2021; Weber et al., 2020). The Chinese government also enforced a series of strict restrictions on travel, transport, manufacture, and constructive activities during the lockdown. Recent studies on the aerosols in China which were conducted during the lockdown period focused on primary emissions and secondary formation, and most of them had revealed changes in aerosol compositions, sources, and processes under a variety of emission control measures (Le et al., 2020; Li et al., 2020; Wang et al., 2020a; Wang et al., 2020c; Zhao et al., 2020; Zheng et al., 2020)."

References

Ibrahim, S., Landa, M., Pešek, O., Pavelka, K., and Halounova, L.: Space-time machine learning models to analyze COVID-19 pandemic lockdown effects on aerosol optical depth over Europe, Remote Sens., 13, 3027, https://doi.org/10.3390/rs13153027, 2021.

Kumar, D., Singh, A. K., Kumar, V., Poyoja, R., Ghosh, A., and Singh, B.: COVID-19 driven changes in the air quality; a study of major cities in the Indian state of Uttar Pradesh, Environ. Pollut., 274, 116512, https://doi.org/10.1016/j.envpol.2021.116512, 2021.

Sanap, S. D.: Global and regional variations in aerosol loading during COVID-19 imposed lockdown, Atmos. Environ., 246, 118132, https://doi.org/10.1016/j.atmosenv.2020.118132, 2021.

Weber, J., Shin, Y. M., Staunton Sykes, J., Archer-Nicholls, S., Abraham, N. L., and Archibald, A. T.: Minimal climate impacts from short-lived climate forcers following emission reductions related to the COVID-19 pandemic, Geophys. Res. Lett., 47, e2020GL090326. https://doi.org/10.1029/2020GL090326, 2020.

Comment (6): Line 112: justify the selection of the factor 2.14.

Response: For the newly developed model AE33 Aethalometer, the optical absorption of aerosols collected on the filter is influenced by scattering of light within the filter. The enhancement of optical absorption is described by the factor C as follows (Weingartner et al., 2003):

$$b_{ATN} = C \times b_{abs} \qquad (R1)$$

where b_{ATN} is the optical attenuation coefficient measured for aerosol particles captured on the filter, and b_{abs} is the in-situ absorption of aerosol particles suspended in the air.

The value of C depends on the filter material, being 2.14 for quartz filter and 1.57 for tetrafluoroethylene-coated glass filter (Drinovec et al., 2015). The quartz filter tape roll (Magee Scientific, USA) was used in the model AE33 in our study campaign; therefore, we have selected the factor of 2.14 to adjust the filter matrix scattering effect accordingly.

References

Weingartner, E., Saathoff, H., Schnaiter, M., Streit, N., Bitnar, B., and Baltensperger, U.: Absorption of light by soot particles: determination of the absorption coefficient by means of aethalometers, J. Aerosol Sci., 34, 1445–1463, https://doi.org/10.1016/S0021-8502(03)00359-8, 2003.

Drinovec, L., Močnik, G., Zotter, P., Prévôt, A. S. H., Ruckstuhl, C., Coz, E., Rupakheti, M., Sciare, J., Müller, T., Wiedensohler, A., and Hansen, A. D. A.: The "dual-spot" Aethalometer: an improved measurement of aerosol black carbon with real-time loading compensation, Atmos. Meas. Tech., 8, 1965–1979, https://doi.org/10.5194/amt-8-1965-2015, 2015.

Comment (7): Line 118: please, discuss about the extinction coefficient uncertainty considering the two different wavelengths for scattering and absorption coefficients.

Response: Based on the Absorption Ångström exponent (AAE) calculated with the power law fitting of light absorption coefficient (b_{abs}) at wavelengths of λ = 370, 470, 520, 590, 660, and 880 nm, b_{abs} at 525 nm can be estimated as follows (Moosmüller et al., 2011):

$$b_{abs}(525\text{ nm}) = b_{abs}(520\text{ nm}) \times \left(\frac{525\text{ nm}}{520\text{ nm}}\right)^{-AAE} \tag{R2}$$

The relative error between $b_{abs}(525\text{ nm})$ and $b_{abs}(520\text{ nm})$ is only $1.5\% \pm 0.1\%$, that is much lower than the relative uncertainty of absorption measurements of model AE33 (5%) (Titos et al., 2015). Thus, the difference of the 5 nm for the b_{abs} can be ignored. To express this point clear, the sentence has been added in Page 5 Line 125–127 in the revised manuscript as "Considering the relative error ($1.5\% \pm 0.1\%$) between b_{abs} at 520 nm and 525 nm is negligible, the amount of b_{ext} in this study was defined as the sum of b_{scat} at 525 nm and b_{abs} at 520 nm."
".

References

Moosmüller, H., Chakrabarty, R. K., Ehlers, K. M., and Arnott, W. P.: Absorption Ångström coefficient, brown carbon, and aerosols: basic concepts, bulk matter, and spherical particles, Atmos. Chem. Phys., 11, 1217–1225, https://doi.org/10.5194/acp-11-1217-2011, 2011.

Titos, G., Lyamani, H., Drinovec, L., Olmo, F. J., Močnik, G., and Alados-Arboledas, L.: Evaluation of the impact of transportation changes on air quality, Atmos. Environ., 114, 19–31, https://doi.org/10.1016/j.atmosenv.2015.05.027, 2015.

Comment (8): Line 135: why to use relative humidity if temperature and dew point include the information of moisture content? Is not redundant? I miss some important and basic meteorological variables such are radiation-related ones. Is there any argument for not to include them? Also, replace 'pressures' by 'pressure'. And a last comment on this sentence. PBLH is retrieved from GDAS data. Which is the method applied to retrieve these values? What is the spatial grid used in these computations?

Response: Thank you for pointing out these points. For the first point, the relative humidity (RH) is redundant since it can be computed from dew point and air temperature. In the revised manuscript, we have removed RH meteorological parameter and performed the generalized additive model (GAM) analysis again.

For the second point, taking radiation-related meteorological data (e.g., solar radiation, land-surface radiation, net radiation, and etc.) as inputs for the GAM model analysis might improve the accuracy of estimation. Unfortunately, we could not be able to collect the synchronous radiation-related meteorological data during the campaign. The GAM constructed in this study by the existing meteorological parameters (wind speed, wind direction, temperature, pressures, dew point, and planetary boundary layer height) was proved to be reasonable and reliable for estimating aerosol light extinction.

Third, the word "pressures" has been replaced by "pressure". Similar errors in Tables S1, S2, and S3 have been also corrected.

Lastly, to obtain the PBLH at the sampling site (34°13' N, 108°52' E) with the GDAS data, linear interpolation was used. We have added the description of the method in Table S1 as "PBLH at the sampling site was obtained using linear interpolation method."

Comment (9): Line 181: what is the advantage of using SBDART instead of other shortwave radiative models such as libRadtran?

Response: The Santa Barbara DISORT Atmospheric Radiative Transfer (SBDART) is a software tool for radiative transfer calculations. All the important processes that affect the ultraviolet, visible, and infrared radiation fields are considered. Its code is a marriage of a sophisticated discrete ordinate radiative transfer (DISORT) module, low-resolution transmission (LOWTRAN) models, and the Mie scattering results, which is well suited for a wide variety of atmospheric radiative energy balances and remote sensing studies (Ricchiazzi et al., 1988). The libRadtran is also a widely used software package for various applications related to atmospheric radiation (Emde et al., 2016; Mayer and Kylling, 2005). Its input options have the same DISORT (Stamnes et al., 2000) and LOWTRAN (Pierluissi and Peng, 1985) as the SBDART, and their reliabilities for estimating the irradiance under different aerosol conditions had been validated (Obregón et al., 2015).

Compared to the SBDART adopting Mie theory applied for the equivalent spherical particle, the libRadtran shows the advantage that six individual habits of ice crystal can be used in the model, including plate, solid column, hollow column, rosette 4, rosette 6, and rough aggregate. With the highly reliable-quality ice crystal information, the libRadtran might reduce the uncertainty in calculating the radiative forcing of the cloud. It is well known that the atmospheric aerosol can perturb the Earth's radiative balance indirectly by acting as cloud condensation nuclei; thus, the libRadtran would be preferred when we study the indirect radiation effect of aerosol in the future.

References

Emd, C., Buras-Schnell, R., Kylling, A., Mayer, B., Gasteiger, J., Hamann, U., Kylling, J., Richter, B., Pause, C., Dowling, T., and Bugliaro, L.: The libRadtran software package for radiative transfer calculations (version 2.0.1), Geosci. Model Dev., 9, 1647–1672, https://doi.org/10.5194/gmd-9-1647-2016, 2016.

Mayer, B. and Kylling, A.: Technical note: The libRadtran software package for radiative transfer calculations - description and examples of use, Atmos. Chem. Phys., 5, 1855–1877, https://doi.org/10.5194/acp-5-1855-2005, 2005.

Obregón, M. A., Serrano, A., Costa, M. J., and Silva, A. M.: Validation of libRadtran and SBDART models under different aerosol conditions, IOP Conf. Ser. Earth Environ. Sci., 28, 12010, https://doi.org/10.1088/1755-1315/28/1/012010, 2015.

Pierluissi, J. H. and Peng, G. S.: New molecular transmission band models for LOWTRAN, Opt. Eng., 24, 541–547, https://doi.org/10.1117/12.945019, 1985.

Ricchiazzi, P., Yang, S. R., Gautier, C., and Sowle, D.: SBDART: A research and teaching software tool for Plane-parallel radiative transfer in the Earth's atmosphere, B. Am. Meteorol. Soc., 79, 2101–2114, https://doi.org/10.1175/1520-0477(1998)079<2101:SARATS>2.0.CO;2, 1998.

Stamnes, K., Tsay, S. C., Wiscombe, W., and Laszlo, I.: DISORT, a general-purpose fortran program for discrete-ordinate-method radiative transfer in scattering and emitting layered media: documentation of methodology, Tech. rep., Dept. of

Physics and Engineering Physics, Stevens Institute of Technology, Hoboken, NJ 07030, 2000.

Comment (10): Line 644: 100 times is missing in this definition of 'change ratio'.
Response: Sorry for the typo, the footnote in Table 1 has been corrected.

Responses to Community #1:

General comments:
This manuscript, titled by The importance of biomass burning in light extinction and direct radiative effect of urban aerosol during the COVID-19 lockdown in China, investigated the impacts of COVID-19 lockdown on aerosol light extinction and direct radiative effect. In fact, many studies have been conducted to explore the impacts of lockdown measures on the aerosol compositions, but how the lockdown measures influenced the aerosol optical property and direct radiative effect is limited. Though the information given in this study has been well known, it is suitable to publish on the Measurement Report. I suggest a major revision of this paper. Before acceptance, some issues must be clarified.

Response: We highly appreciate the thoughtful and valuable suggestions. We have revised the manuscript accordingly, which has been significantly improved. Besides, the language has been also polished by a native English speaker. Please refer to our point-point responses as follow.

Comment (1): The contributions of biomass burning to aerosol b_{ext} and DRF increased during lockdown period in this study which just focused on only one site. How did you find out that the importance of control biomass burning for tackling climate change in China? More evidence in the other region should be provided to make your conclusion robust.

Response: Our manuscript focused on a study case in Xi'an, China. Therefore, we do agree with the point that it is inappropriate to conclude the importance of controlling biomass burning for tackling climate change throughout the entire of China. Actually, biomass burning is an important anthropogenic source of aerosol in many Chinese cities, such as Tianjin (Khan et al., 2021), Jinan (Cheng et al., 2021), Guangzhou (Huang et al., 2018), Chengdu (Li et al., 2017), and etc. The results and conclusions of this case study could be a significant reference to other cities in China, where the air is greatly polluted by biomass burning. To address this point clear, we made some changes in the revised manuscript as follows:

(1). The title has been revised to specify the location of this case study. It now reads: "Measurement report: The importance of biomass burning in light extinction and direct radiative effect of urban aerosol during the COVID-19 lockdown in Xi'an, China"

(2). To illustrate the importance of controlling biomass burning in China, the sentences have been added in Section 3.5. Page 12 Line 330–335: "Similar to Xi'an city, the pollution sources of traffic and biomass burning were the two most significant anthropogenic sources of aerosol in most Chinese cities, such as Chengdu, Guangzhou, Jinan, Tianjin, and etc (Cheng et al., 2021; Huang et al., 2018; Khan et al., 2021; Li et al., 2017b). The results in this study indicated that the control measures on traffic in the lockdown were highly effective for mitigating the effects of climate change in the short term, while future emission control policies should consider the importance of biomass burning to tackle climate change in China."

References

Cheng, M. T., Tang, G. Q., Lv, B., Li, X. R., Wu, X. R., Wang, Y. M., and Wang, Y. S.: Source apportionment of $PM_{2.5}$ and visibility in Jinan, China, J. Environ. Sci., 102, 207–215, https://doi.org/10.1016/j.jes.2020.09.012, 2021.

Huang, X. F., Zou, B. B., He, L. Y., Hu, M., Prévôt, A. S. H., and Zhang, Y. H.: Exploration of $PM_{2.5}$ sources on the regional scale in the Pearl River Delta based on ME-2 modeling, Atmos. Chem. Phys., 18, 11563–11580, https://doi.org/10.5194/acp-18-11563-2018, 2018.

Khan, J. Z., Sun, L., Tian, Y. Z., Shi, G. L., and Feng, Y. C.: Chemical characterization and source apportionment of PM_1 and $PM_{2.5}$ in Tianjin, China: Impacts of biomass burning and primary biogenic sources, J. Environ. Sci., 99, 196–209, https://doi.org/10.1016/j.jes.2020.06.027, 2021.

Li, L. L, Tan, Q. W., Zhang, Y. H., Feng, M., Qu, Y., An, J. L., and Liu, X. G.: Characteristics and source apportionment of $PM_{2.5}$ during persistent extreme haze events in Chengdu, southwest China, Environ. Pollut., 230, 718–729, https://doi.org/10.1016/j.envpol.2017.07.029, 2017.

Comment (2): Many studies have proved that sulfate can emitted from coal combustion, especially in the regions where a great deal of coal consumed every year, such as Xi'an. Thus, is it proper to regard sulfate as the secondary source?

Response: In fact, coal consumption in Xi'an had a dramatic reduction over the last decade. Even though the coal combustion could emit sulfate directly (Tian et al. 2018), most sulfate in Xi'an formed from secondary atmospheric reaction. Xing et al. (2020) reported that the secondary sulfate accounted for 74.5% of the total sulfate in Xi'an, which is consistent with our source apportionment result. In this study, the average sulfate from the two secondary sources (i.e., nitrate plus SOA source and sulfate plus SOA source) accounted for 74.2% of the total sulfate in Xi'an. Therefore, sulfate here is reasonably regarded as secondary source in Xi'an.

References

Tian, J., Ni, H. Y., Han, Y. M., Shen, Z. X., Wang, Q. Y., Long, X., Zhang, Y., and Cao, J. J.: Primary $PM_{2.5}$ and trace gas emissions from residential coal combustion: Assessing semi-coke briquette for emission reduction in the Beijing-Tianjin-Hebei region, China, Atmos. Environ., 191, 378–386, https://doi.org/10.1016/j.atmosenv.2018.07.031, 2018.

Xing, M., Liu, W., Li, X., Zhou, W., Wang, Q., Tian, J., Li, X., Tie, X., Li, G., Cao, J., Bao, H., and An, Z.: Vapor isotopic evidence for the worsening of winter air quality by anthropogenic combustion-derived water, P. Natl. Acad. Sci. USA., 117(52), 33005–33010, https://doi.org/10.1073/pnas.1922840117, 2020.

Comment (3): Some important references about aerosol optical property have not been cited in this study, such as Xu et al., 2020, ESTL, Liu et al., 2020, GRL and Yao et al., 2021, npj CAS. I think these articles may improve your Introduction and discussion.

Response: Thanks for the useful references. These important articles (Liu et al., 2020; Xu et al., 2020; Yao et al., 2021) have been added to the main manuscript as follows:

(1). Page 11 Line 318–320: "The mean aerosol $DRE_{atmosphere}$ decreased from 31.0 ± 23.2 W m^{-2} before the lockdown to 14.1 ± 11.5 W m^{-2} in the lockdown, with a reduction of 54.5%. This can be explained by the reduced aerosol concentration and increased SSA (Liu et al., 2020)."

(2). Page 8 Line 209–213: "The mean values of b_{scat}, b_{abs}, and b_{ext} during the normal period were 688.1 ± 261.4 Mm^{-1}, 86.6 ± 43.0 Mm^{-1}, and 774.7 ± 298.1 Mm^{-1}, respectively, which are consistent with the values (657.4 ± 436.9 Mm^{-1}, 104.0 ± 69.6 Mm^{-1}, and 761.4 ± 506.5 Mm^{-1}) reported previously in winter of 2009 in Xi'an (Cao et al., 2012), even though a series of nationwide air quality standards and long-term pollution control policies have been implemented in the 74 major cities since 2013 (Xu et al., 2020b; Zheng et al., 2018)."

(3). Page 2 Line 49–54: "The spatiotemporal variations of aerosol optical properties (e.g., light scattering coefficient (b_{scat}), light absorption coefficient (b_{abs}), light extinction coefficient (b_{ext}), and single scattering albedo (SSA)) highly depended on their chemical compositions and sources (Malm and Hand, 2007; Tao et al., 2014; Yao et al., 2021), can elevate uncertainties in estimating aerosol DRE (IPCC, 2013; Ma et al., 2012)."

References

Liu, D. T., Hu, K., Zhao, D. L., Ding, S., Wu, Y. F., Zhou, C., Yu, C. J., Tian, P., Liu, Q., Bi, K., Wu, Y. Z., Hu, B., Ji, D. S., Kong, S. F., Ouyang, B., He, H., Huang, M. Y., and Ding, D. P.: Efficient vertical transport of black carbon in the planetary boundary layer, Geophys. Res. Lett., 47, e2020GL088858, https://doi.org/10.1029/2020GL088858, 2020.

Xu, W. Y., Kuang, Y., Bian, Y. X., Liu, L., Li, F., Wang, Y. Q., Xue, B., Luo, B., Huang, S., Yuan, B., Zhao, P. S., and Shao, M.: Current challenges in visibility improvement in southern China, Environ. Sci. Technol. Lett., 7, 395–401, https://doi.org/10.1021/acs.estlett.0c00274, 2020.

Yao, L. Q., Kong, S. F., Zheng, H., Chen, N., Zhu, B., Xu, K., Cao, W. X., Zhang, Y., Zheng, M. M., Cheng, Y., Hu, Y., Zhang, Z. X., Yan, Y. Y., Liu, D. T., Zhao, T. L., Bai, Y. Q., and Qi, S. H.: Co-benefits of reducing PM$_{2.5}$ and improving visibility by COVID-19 lockdown in Wuhan, NPJ Clim. Atmos. Sci., 4, 40, https://doi.org/10.1038/s41612-021-00195-6, 2021.

Comment (4): Line 30 "importance of biomass burning for tackling climate change" is "importance of control biomass burning for tackling climate change" ?

Response: Change made. Page 1 Line 30–32: "Our study provides insights into aerosol b_{ext} and DRE from anthropogenic sources, and the results implied the importance of controlling biomass burning for tackling climate change in China in the future."

Comment (5): The mass and optical property closure should be conducted after the source apportionment.

Response: As shown in Figures R1 and R2 (also referred to Figures S10 and S11), both the mass and optical property closure have been conducted for the source apportionment. In the revised manuscript, the relevant description has been revised. Page 10 Line 268–269: "The six-factor solution was selected to be the optimal solution, which can adequately account for the variability in PM$_{2.5}$ mass concentration and optical coefficients (Figures S10 and S11)."
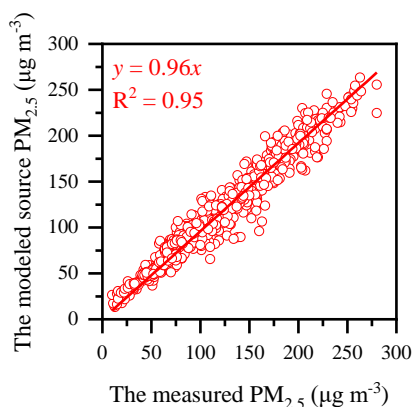

Figure R1. Linear relationship between the modeled source and the measured PM$_{2.5}$ mass concentration. The modeled source PM$_{2.5}$ was strongly correlated linearly with the measured optical PM$_{2.5}$ (R^2 = 0.95, slope = 0.96), indicating that the six identified sources can adequately account for the variability in PM$_{2.5}$ mass concentration.
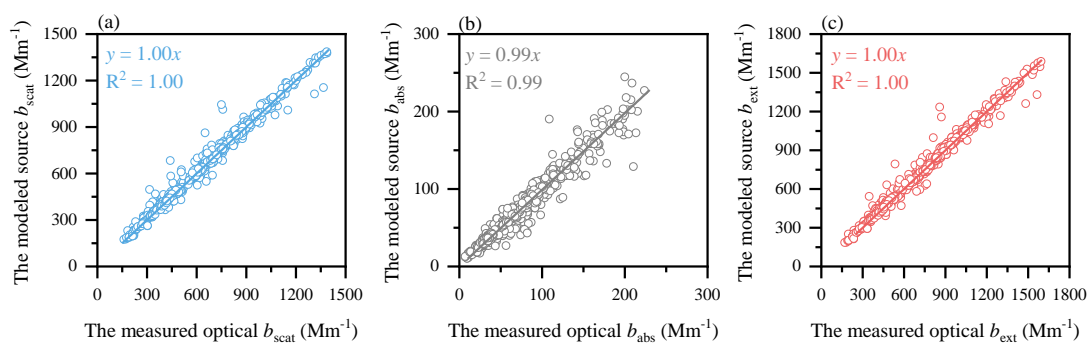
Figure R2. Linear relationships between the modeled source and the measured optical (a) b_{scat}, (b) b_{abs}, and (c) b_{ext}. The modeled source b_{scat}, b_{abs}, and b_{ext} were strongly correlated linearly with the measured optical b_{scat} (R^2 = 1.00, slope = 1.00), b_{abs} (R^2 = 0.99, slope = 0.99), and b_{ext} (R^2 = 1.00, slope = 1.00), indicating that the six identified sources can adequately account for the variability in aerosol optical coefficients.

Comment (6): Some details such as line 201 "which is" or "which are", should be checked carefully.
Response: Corrected.

Measurement report: The importance of biomass burning in light extinction and direct radiative effect of urban aerosol during the COVID-19 lockdown in Xi'an, China

Jie Tian[1,2], Qiyuan Wang[1,2,3], Huikun Liu[1], Yongyong Ma[4], Suixin Liu[1,2], Yong Zhang[1], Weikang Ran[1], Yongming Han[1,2,3], and Junji Cao[5]

[1]State Key Laboratory of Loess and Quaternary Geology, Institute of Earth Environment, Chinese Academy of Sciences, Xi'an 710061, China
[2]CAS Center for Excellence in Quaternary Science and Global Change, Xi'an 710061, China
[3]~~Guanzhong Plain Ecological Environment Change and Comprehensive Treatment~~ National Observation and Research Station of Regional Ecological Environment Change and Comprehensive Management in the Guanzhong Plain, Shaanxi, Xi'an 710061, China
[4]Meteorological Institute of Shaanxi Province, Xi'an 710015, China
[5]Institute of Atmospheric Physics, Chinese Academy of Sciences, Beijing 100029, China

Correspondence: Qiyuan Wang (wangqy@ieecas.cn) and Junji Cao (jjcao@mail.iap.ac.cn)

Abstract. ~~To mitigate climate change in China~~Due to the complexity of emission sources, a better understanding of aerosol optical properties ~~of aerosol~~ is required ~~due~~ to ~~mitigate climate change in China~~the complexity in emission sources. Here, an intensive real-time measurement was conducted in an urban area of China before and during the lockdown of Coronavirus Disease 2019 (COVID-19), to explore the impacts of anthropogenic activities on aerosol light extinction and direct radiative effect (DRE). The mean light extinction coefficient (b_{ext}) reduced from 774.7 $\pm$298.1 Mm^{-1} during the normal period to 544.3 $\pm$179.4 Mm^{-1} during the lockdown period. The generalized addictive model analysis indicated that the large decline of b_{ext} (29.7%) was ~~entirely~~ attributed to the sharp reductions in anthropogenic emissions. Chemical calculation of b_{ext} based on the ridge regression analysis showed that organic aerosol (OA) was the largest contributor to b_{ext} in both periods (45.1–61.4%), and contributions of two oxygenated OAs to b_{ext} increased by 3.0–14.6% during the lockdown. A hybrid environmental receptor model combining with chemical and optical variables identified six sources of b_{ext}. It was found that b_{ext} from traffic-related emission, coal combustion, fugitive dust, nitrate plus secondary OA (SOA) source, and sulfate plus SOA source decreased by 21.4–97.9% in the lockdown, whereas b_{ext} from biomass burning increased by 27.1% mainly driven by undiminished needs of residential cooking and heating. The atmospheric radiative transfer model was further used to illustrate that biomass burning instead of traffic-related emission became the largest positive effect (10.0 $\pm$10.9 W m^{-2}) on aerosol DRE in the atmosphere during the lockdown. Our study provides insights into aerosol b_{ext} and DRE from anthropogenic sources, and the results implied the importance of controlling biomass burning for tackling climate change in China in the future.

1 Introduction

The abrupt outbreak of Coronavirus Disease 2019 (COVID-19) ~~since December of 2019~~ caused unprecedented economic and social disruption (Yao et al., 2020). Most worldwide countries implemented the city lockdown to curb the virus spread among humans, providing a rare opportunity to investigate the impacts of anthropogenic activities on the air quality (Ibrahim et al., 2021; Kumar et al., 2021; Sanap, 2021; Weber et al., 2020). The Chinese government also enforced ~~implemented the city lockdown and~~ a series of strict restrictions on travel, transport~~s~~, manufacture~~factories~~, and constructive activities during the lockdown~~for numerous cities in China to curb the virus spread among humans.~~ ~~This provides a rare opportunity to investigate the impacts of anthropogenic activities on air pollution in China~~. Recent ~~aerosol~~ studies on the aerosols in China which were~~are~~ conducted during the lockdown period~~with a major~~ focused~~ on~~ primary emissions and secondary formation, and most of them had~~ve~~ revealed changes in aerosol compositions, sources, and processes under a variety of emission control measures (Le et al., 2020; Li et al., 2020; Wang et al., 2020a; Wang et al., 2020c; Zhao et al., 2020; Zheng et al., 2020). However, only a few studies were~~a~~ conducted to explore the link of chemical constituents in aerosol with light absorption during the lockdown (Chen et al., 2020; Lin et al., 2021; Xu et al., 2020a). The influences of reduced anthropogenic activities on the variations of aerosol optical properties and direct radiative effect (DRE) are less understood.

Atmospheric aerosols alter the radiative energy budget by directly scattering and absorbing solar and terrestrial radiation to affect global~~the globe~~ climate change (Bellouin et al., 2013; Yao et al., 2017). The spatiotemporal variations of aerosol optical properties (e.g., light scattering coefficient (b_{scat}), light absorption coefficient (b_{abs}), light extinction coefficient (b_{ext}), and single scattering albedo (SSA)) ~~that~~ highly depended on their chemical compositions and sources (Malm and Hand, 2007; Tao et al., 2014; Yao et al., 2021), can ~~result in~~elevate uncertainties in estimating aerosol DRE (IPCC, 2013; Ma et al., 2012). Therefore, distinguishing chemical composition- and source-specific aerosol optical properties from a mixture of aerosols in the atmosphere would make a better understanding of the climate change during the COVID-19 lockdown.

The relationship between aerosol optical coefficients and chemical compositions can be built by the Interagency Monitoring of Protected Visual Environments algorithm and multiple linear regression (MLR) (Deng et al., 2016; Malm and Hand, 2007; Shen et al., 2014; Tao et al., 2014, 2015). However, previous studies often regarded organic aerosol (OA) as a whole light scattering component only. In reality, ~~there are~~ some OA components can absorb light, which is collectively termed as brown carbon (BrC) (Andreae and Gelencsér, 2006). The DRE caused by BrC has been reported to be nonnegligible (e.g., 0.04 W m^{-2} to 0.57 W m^{-2}) (Feng et al., 2013; Lin et al., 2014; Wang et al., 2014). Furthermore, the optical properties of OA can vary widely due to the complexity of OA components associated with primary sources, formation pathways, and aging processes (Laskin et al., 2015). For instance, primary OA (POA) from anthropogenic

2

sources (e.g., biomass burning and coal combustion) usually has different mass scattering and absorption efficiencies (MSE and MAE) in the atmosphere compared to secondary OA (SOA) formed though photochemical or aqueous-phase oxidations (Han et al., 2015; Qin et al., 2018). Therefore, investigating POA and SOA contributions to aerosol light scattering and absorption would reduce uncertainties in the chemical apportionment of aerosol optical properties.

Previous studies have been conducted on the aerosol optical source apportionment. According to the multi-wavelength aethalometer measurement, the source of aerosol b_{abs} can be investigated by exploiting the differences in absorption spectra of light-absorbing materials (Herich et al., 2011; Sandradewi et al., 2008; Zotter et al., 2017). In this method, the aerosol absorption near-ultraviolet and short-visible regions of the spectrum from biomass burning are~~is~~ assumed to be enhanced because of BrC emitted, compared to that from fossil fuel combustion (Kirchstetter et al., 2004; Tian et al., 2019). This makes it possible to derive their contributions to light absorption by using the specific source absorption Ångström exponent (AAE), but the so-called "aethalometer model" could not distinguish as many sources resolved by receptor models due to the similar optical properties of the aerosol sources (Saarikoski et al., 2021). In contrast, receptor models can be utilized to resolve multiple optical source apportionment of aerosol. Several studies used a combination of the receptor model and MLR to indirectly identify sources of aerosol b_{scat}, b_{abs}, and b_{ext} (Cao et al., 2012; Tian et al., 2020; Zhou et al., 2017). For example, Zhou et al. (2017) firstly used positive matrix factorization analysis to quantify the mass contributions of aerosol from secondary aerosol, biomass burning, traffic-related emissions, and coal combustion~~burning~~ based on the sole chemical species, and then the MLR was used to apportion the contribution of each source to b_{scat} and b_{abs}. In addition, recent studies have attempted to conduct direct optical source apportionment by combining aerosol chemical species with optical coefficients in one receptor model (Forello et al., 2019; ~~Q.~~ Wang et al., 2020b; Xie et al., 2019). This promising method can provide both chemical and optical profiles in each source to improve the performance of source identification, and may eliminate potential uncertainties caused by the indirect approach.

The Fenwei Plain is designated as the key region~~s~~ of pollution treatment in the "T~~t~~hree-year action plan to fight air pollution" implemented by the Chinese State Council in 2018. As one of the megacities in this plain, Xi'an has been facing severe air pollution problem, especially in winter (Niu et al., 2016; Wang et al., 2015). Here, we conducted high~~ly~~ time-resolved aerosol b_{scat} and b_{abs} measurements in Xi'an before and during the city lockdown in China. The main objectives are to (1) characterize the changes of aerosol optical properties since COVID-19 lockdown; (2) quantify the contributions of individual chemical composition and specific source to b_{ext}; and (3) evaluate source-specific aerosol DRE based on a radiative transfer model. This study provides insights into the response of aerosol b_{ext} and DRE to anthropogenic emission sources, which is a scientific basis for establishing~~making~~ future emission control policies to deal with climate change in China.

2 Methodology

95 **2.1 Sampling site and period**

Intensive measurements of aerosol optical properties were conducted at ~~an~~ one urban sampling site ~~located at~~ of ~~the~~ ~~Guanzhong Plain Ecological Environment Change and Comprehensive Treatment~~ National Observation and Research Station of Regional Ecological Environment Change and Comprehensive Management in the Guanzhong Plain, southwest of Xi'an downtown (34°13' N, 108°52' E, Figure S1). All instruments were placed at the rooftop of an office

100 building (~ 10 m above the ground) and approximately 30 m from the nearest traffic road. A ~~D~~detailed description of the sampling site can be found in Tian et al. (2021). In this study, the sampling campaign consisted of two distinct periods: normal period (~~1 to 23~~ January 1st to 23rd, 2020) and COVID-19 lockdown period (~~27~~ January 27th to ~~7~~ February 7th, 2020). Three days of ~~24 to 26~~ January 24th–26th, 2020 were excluded due to the intensive influence of fireworks for the Chinese New Year celebration.

105 **2.2 Measurements**

2.2.1 Real-time measurements of b_{scat} and b_{abs}

A single wavelength integrating nephelometer (Aurora 1000, Ecotech, Melbourne, Australia) was carried out to measure aerosol b_{scat} at a wavelength of 525 nm with a 5-min time resolution. In the measurement volume, the ambient air sampled with a flow rate of 5 L min^{-1} was illuminated by the light source, that only light scattered at scattering angles between

110 10 ° and 170 ° can reach~~ed~~ the photomultiplier tube. Thereafter, b_{scat} can be calculated by the proportion of the electrical signals produced by the photomultiplier tube. Span calibration was made using CO_2 to ensure the accuracy of the instrument before sampling, and zero calibration w~~ere~~as performed twice each day with particle-free air to subtract the Rayleigh scattering. More detailed principles of the Aurora 1000 have been described ~~in~~ elsewhere (Chamberlain-Ward and Sharp, 2011).

115 Aerosol b_{abs} at wavelengths of 370 nm, 470 nm, 520 nm, 590 nm, 660 nm, and 880 nm were measured by a newly developed Aethalometer (model AE33, Magee Scientific, Berkeley, CA, USA) with a 1-min time resolution. Briefly, the model AE33 was the filter-based absorption photometer that simultaneously measured the light attenuation transmitted through two parallel spots of the aerosol filter with 3.85 L min^{-1} and 1.15 L min^{-1}, respectively. Based on "dual-spot" measurements, it used a real-time loading effect compensation algorithm to eliminate the nonlinear loading effect ~~as~~by

120 increasing the deposition amount of aerosol on the filter. Additionally, a factor of 2.14 was used in the model AE33 to automatically modify the quartz filter matrix scattering effect. A detailed description of this instrument can be found in Drinovec et al. (2015).

4

Both of the Aurora 1000 and model AE33 instruments equipped with a $PM_{2.5}$ cyclone separator in the sampling inlet to remove particles larger than 2.5 μm, and a Nafion® dryer (MD-700-24S, Perma Pure, Inc., Lakewood, NJ, USA) to

125 retain particles (relative humidity < 40%) before entering these instruments. Considering the relative error (1.5% ±0.1%) between b_{abs} at 520 nm and 525 nm is negligible, tThe amount of b_{ext} in this study was defined as the sum of b_{scat} at 525 nm and b_{abs} at 520 nm.

2.2.2 Complementary data

A quadrupole aerosol chemical speciation monitor (Q-ACSM, Aerodyne Research Inc., Billerica, Massachusetts, USA)

130 and a Xact 625 ambient metals monitor (Xact 625i, Cooper Environmental Services, Beaverton, OR, USA) were operated to obtain chemical composition characteristics (Furger et al., 2020; Ng et al., 2011). The Q-ACSM measured concentrations of non-refractory species in PM_1 (NO_3^-, SO_4^{2-}, NH_4^+, Cl^-, and OA), and OA was further resolved into POA, less-, and more-oxidized oxygenated OA (LO-OOA and MO-OOA). Detailed information on the Q-ACSM data process and source apportionment of OA can be found in our previous paper (Tian et al., 2021). The Xact 625i quantified

135 hourly element concentrations through X-ray fluorescence analysis, including Si, K, Ca, Cr, Mn, Fe, Zn, As, Se, Ba, Hg, and Pb. Additionally, BC concentration was calculated using b_{abs} at 880 nm (Kirchstetter et al., 2004). Online $PM_{2.5}$ and NO_x concentrations were obtained from the Department of Ecology and Environment of Shaanxi Province. More detailed descriptions of these complementary data can be found in Table S1.

2.3 Meteorological conditions separation

140 A generalized addietive model (GAM) combined with integrated smoothness estimation was used to establish the relationship between b_{ext} and several meteorological parameters as follows (Wood, 2004):

$$\ln b_{ext}(i) = \sum_{j=1}^{7} f_j(MP_j(i)) + \beta_0 + e_i \tag{1}$$

where $b_{ext}(i)$ is the b_{ext} in Mm^{-1} averaged over the ith hour; MP_j represents the jth meteorological parameter, such as wind speed, wind direction, relative humidity, temperature, pressures, dew point, and planetary boundary layer height, where

145 the data sources can be found in Table S1; f corresponds to the smooth function describing the association between b_{ext} and meteorological parameters; β_0 is the model intercept; and e_i is the regression residuals which is assumed to be normally distributed.

Based on the R package "mgcv" (Wood, 2017), the whole campaign dataset was divided into three parts: a model data (80% of data during the normal period) for establishing the b_{ext} GAM, a test data (20% of data during the normal period)

150 for verifying the accuracy of the model, and a forecast data (100% of data during the lockdown period) for estimating the contributions of meteorological conditions and emissions on b_{ext} reduction.

2.4 Chemical calculation of b_{scat} and b_{abs}

BecauseIn view of POA and SOA with nonnegligible light scattering and absorbing abilities, the amount of b_{scat} and b_{abs} associated with individual chemical species can be estimated statistically using the ridge regression method:

$$b_{scat} = a_1[NH_4NO_3] + a_2[(NH_4)_2SO_4] + a_3[\text{fine soil}]$$
$$+ a_4[POA] + a_5[\text{LO-OOA}] + a_6[\text{MO-OOA}] + c_1 \tag{2}$$

$$b_{abs} = b_1[BC] + b_2[POA] + b_3[\text{LO-OOA}] + b_4[\text{MO-OOA}] + c_2 \tag{3}$$

where b_{scat} and b_{abs} are given in unit of Mm^{-1}; the bracket notation [] represents the specific chemical species concentration in $\mu g\ m^{-3}$; the a_i and b_i ($i = 1$–6) describe the MSE and MAE of each chemical species in the unit of $m^2\ g^{-1}$, respectively; and c_i ($i = 1$ or 2) is the constant. In equation (2), the concentrations of $[NH_4NO_3]$, $[(NH_4)_2SO_4]$, and [fine soil] were calculated using $1.29 \times [NO_3^-]$, $1.35 \times [SO_4^{2-}]$, and $[Fe]/0.032$, respectively (Chow et al., 2015; CNEMC, 1990). In equation (3), b_1 was calculated by the absorption Ångström exponent method, and the detailed description can be seen in Text S1.

2.5 Hybrid environmental receptor model (HERM) for source apportionment

The source apportionment of b_{ext} was performed with HERM which is a newly developed bilinear model (Chen and Cao, 2018). Briefly, the HERM solves non-negative matrices of unknown factor profiles and contributions with a pre-set number of factors K by iteratively minimizing the object function Q defined as follows:

$$Q = \sum_{j=1}^{J} \sum_{i=1}^{I} \frac{\left(x_{ij} - \sum_{k=1}^{K} g_{ik} f_{kj}\right)^2}{\sigma_{x_{ij}}^2 + \sum_{k=1}^{K}\left(g_{ik}^2 \sigma_{f_{kj}}^2 + \delta_{ik}\sigma_{x_{ij}}^2\right)} \tag{4}$$

where I, J, and K are the number of samples, aerosol variables, and factors, respectively; the indices of i, j, k represent the sample, aerosol variable, and factor, respectively; x_{ij} is the measured ambient data spectral matrix; f_{kj} is the factor profile matrix; g_{ik} is factor contribution matrix; $\sigma_{x_{ij}}$ and $\sigma_{f_{kj}}$ represent the error in measured ambient data and variability in constrained factor profile, respectively; δ_{ik} is set to 0 or 1 depending on whether the kth factor profile is constrained or unconstrained, respectively.

In this study, both chemical species (PM$_{2.5}$, NO$_3^-$, SO$_4^{2-}$, NH$_4^+$, Cl$^-$, BC, POA, LO-OOA, MO-OOA, Si, K, Ca, Cr, Mn, Fe, Zn, As, Se, Ba, Hg, and Pb in $\mu g\ m^{-3}$) and optical variables (b_{scat} and b_{abs} in Mm^{-1}) were used as input data for the HERM analysis. The uncertainties of hourly ambient data except elements were introduced by the standard deviation of samples with higher time resolution (< 1-hour); the uncertainty of the element was estimated using its concentration, the default analytical relative error (10%) (Rai et al., 2020), and method detection limit (MDL) (Norris et al., 2014) (Text

S2). All input variables were classified as strong due to the high signal-to-noise (SNR > 2). Here, the HERM had
180   predetermined: (1) the ith sample was excluded from source apportionment when missing values occurred in variables;
(2) PM$_{2.5}$ value in factor profile was set to unity as a reference standard for both chemical and optical variables.

A range of factor numbers from two2 to eight8 was selected to run in the HERM software with completely unconstrained
factor profiles, and diagnostic plots are detailed in the supplementary material (Text S3 and Figures S2–S7). The six6-
factor solution without mixed source was found to be the optimal solution based on multiple criteria including (1)
185   variations in Q/Q$_{exp}$ that can be used as a metric for choosing the best number of resolved factors (Ulbrich et al., 2009);
(2) physical meaningfulness of distinct factor profiles and explained variations (EV) of variables; (3) agreement between
the measured and modeled values; and (4) good correlations with external and internal tracers. Detailed information on
the final selected factor profiles and contributions are presented in Section 3.4.

2.6 DRE calculations

190   The Santa Barbara DISORT Atmospheric Radiative Transfer (SBDART) developed by the Institute for Computational
Earth System Science, University of California was utilized to estimate the source-specific aerosol DRE. It can calculate
the downwelling and upwelling radiative flux (F$_{down}$ and F$_{up}$), in which the difference indicates the net radiative flux (ΔF
= F$_{down}$ — F$_{up}$). A detailed description of the SBDART can be found in Ricchiazzi et al. (1998). Based on the optical
source apportionment results, the SBDART model input values of aerosol optical depth, SSA, asymmetry factor, and
195   optical coefficients were retrieved using the Optical Properties of Aerosol and Cloud (OPAC) model (Hess et al., 1998).
The aerosol DRE can be calculated as follows:

$$DRE_{atmosphere} = DRE_{top} - DRE_{surface} \tag{5}$$

$$DRE_{top} = \Delta F_{top}(\text{with aerosol}) - \Delta F_{top}(\text{without aerosol}) \tag{6}$$

$$DRE_{surface} = \Delta F_{surface}(\text{with aerosol}) - \Delta F_{surface}(\text{without aerosol}) \tag{7}$$

200   where the indices of atmosphere, top, and surface indicate the DRE in the atmosphere, at the top of the atmosphere, and
the earth's surface, respectively; ΔF(with aerosol) and ΔF(without aerosol) represent the net radiative flux with and
without aerosol, respectively.

3 Results and discussion

3.1 General descriptions of aerosol optical properties

205   The temporal variations of hourly mean b_{scat}, b_{abs}, b_{ext}, and SSA together with $PM_{2.5}$ mass concentrations for the entire sampling period are depicted in Figure ~~S8~~1, while a statistics summary of optical and chemical parameters during the normal and COVID-19 lockdown periods is shown in Table 1. The optical coefficients decreased dramatically in accord with the significant reduction of $PM_{2.5}$ since stringent control measures on emission sources were implemented during the lockdown period (Tian et al., 2021; Zheng et al., 2020). The mean values of b_{scat}, b_{abs}, and b_{ext} during the normal

210   period were 688.1 $\pm$ 261.4 Mm^{-1}, 86.6 $\pm$ 43.0 Mm^{-1}, and 774.7 $\pm$ 298.1 Mm^{-1}, respectively, which are~~is~~ consistent with the values (657.4 $\pm$ 436.9 Mm^{-1}, 104.0 $\pm$ 69.6 Mm^{-1}, and 761.4 $\pm$ 506.5 Mm^{-1}) reported previously in winter of 2009 in Xi'an (Cao et al., 2012), even though a series of nationwide air quality standards and long-term pollution control policies have been implemented in the 74 major cities since 2013 (Xu et al., 2020b; Zheng et al., 2018). Comparatively, the kind of control measures aiming to curb the outbreaks did not last long, but it was unprecedentedly strictest in China. The

215   large decreases (27.6–47.0%) were found in b_{scat}, b_{abs}, and b_{ext} in the lockdown (498.4 $\pm$ 159.0 Mm^{-1}, 45.9 $\pm$ 22.9 Mm^{-1}, and 544.3 $\pm$ 179.4 Mm^{-1}, respectively), providing insights into the role of anthropogenic emissions on aerosol optical properties.

The SSA defined as the ratio of b_{scat} to b_{ext} increased from 0.89 $\pm$ 0.03 during the normal period to 0.92 $\pm$ 0.02 during the lockdown period. As presented in Figure ~~S9a~~ 2a and b, SSA showed linear increases with the mass fractions of

220   secondary inorganic aerosol (SIA = NH_4NO_3 + $(NH_4)_2SO_4$) to $PM_{2.5}$ (R^2 = 0.83–0.84) and SOA (SOA = LO-OOA + MO-OOA) to OA (R^2 = 0.94–0.99), indicating an enhanced role of secondary formation in the lockdown. In addition, the correlations of SSA and the ratio of LO-OOA to MO-OOA were established to reveal a more complex influence of SOA on SSA (Figure ~~S9c~~2c), which showed ~~obviously~~ negative relationships (R^2 = 0.69–0.79). It indicated that SSA can be impacted by the degree of oxidation on aerosol, and higher scattering and lower absorption abilities are usually

225   found for more oxidized OA (Han et al., 2015; Lee et al., 2014).

3.2 Effects of emission reduction and meteorological conditions on reduced b_{ext}

Figure ~~1~~3 shows the time series of the measured and GAM-predicted b_{ext} for the model data, test data, and forecast data. As shown in Tables S2 and S3, the constructed GAM with adjusted R^2 value (0.54~~69~~) can explain 54~~6.9~~% of the variation in b_{ext} after incorporating the nonlinear relationships between optical and meteorological parameters. Independent

230   smoothed meteorological variables of the model were statistically significant by according to p values (< 0.05) from F test. Concurvity indices between each independent smoothed parameter were within 0.5, indicating there was no serious multicollinearity (Schimek, 2009).

Before applying the constructed GAM to predict the b_{ext} during the lockdown period, the cross-validation test was used to evaluate the model. For the test data (20% of data during the normal period), the R^2 value of the linear regression and

235 index of agreement (IOA) (Wu et al., 2018) between the measured and GAM-predicted b_{ext} was 0.~~80~~ 83 and 0.~~91~~92, respectively, suggesting a good performance of the constructed GAM. T~~herefore, t~~he difference between the measured and GAM-predicted b_{ext} in the lockdown can be attributed to emission reduction through the implementation of stringent control measures on emission sources. The emission reduction decreased b_{ext} by 29~~9~~4.~~2~~6 Mm^{-1} during the lockdown period, higher than the decline of measured b_{ext} (230.4 Mm^{-1}) from normal to lockdown periods. It is indicated that the

240 meteorological conditions enhanced b_{ext} by 6~~8~~4.~~8~~2 Mm^{-1} during the lockdown period, further reflecting the effective control of anthropogenic emissions.

3.3 Contribution of chemical components to b_{ext}

Table 2 presents the estimated MSE and MAE of an individual chemical component during the normal and lockdown periods. The MSEs of NH$_4$NO$_3$ (3.74 ±0.18 m^2 g^{-1}) and (NH$_4$)$_2$SO$_4$ (7.35 ±0.25 m^2 g^{-1}) during the normal period were

245 higher than those (3.23 ±0.18 m^2 g^{-1} and 4.78 ±0.35 m^2 g^{-1}) during the lockdown period. This may be explained by the higher mass loadings and peak diameters of aerosol without control measures (Cheng et al., 2015; Tao et al., 2015). The MAE of BC decreased from 15.00 m^2 g^{-1} to 13.27 m^2 g^{-1} ~~that~~ related to the decline of AAE of BC (Text S1). The MSEs and MAEs of OA factors varied widely, from 3.48 m^2 g^{-1} to 12.89 m^2 g^{-1} and from 0.25 m^2 g^{-1} to 0.59 m^2 g^{-1}, respectively, due to the complex chemical variability of OA constituents (Hallquist et al., 2009; Moise et al., 2015). The scattering

250 ability of OA increased with oxidation level (from POA to MO-OOA) (Cappa et al., 2011; Flores et al., 2014); however, the dependence on oxidation level of OA MAEs presented a more complex trend. LO-OOA had ~~the~~ higher MAE values than those of POA, indicating more BrC chromophores with stronger light-absorbing capacity formed under less-oxidized condition (Zhang et al., 2020). Additionally, the effect of photo-bleaching in the atmosphere that can weaken the light absorption ability of BrC ~~that~~ resulted in the reduction of MO-OOA MAEs (Wang et al., 2021).

255 Chemical calculation of b_{ext} was confirmed to be a reasonable estimation of aerosol optical coefficients by using chemical components data (Figures S8~~10~~ and S9~~11~~). As shown in Figure 2~~4~~, OA (POA + LO-OOA + MO-OOA) was the largest contributor to b_{ext} in both periods, accounting for 45.1–61.4%, followed by NH$_4$NO$_3$ (16.5–24.1%), BC (9.3–13.1%), (NH$_4$)$_2$SO$_4$ (7.9–11.2%), and fine soil (4.9–6.5%). This result was different from previous findings that SIA was often the largest contributor to b_{ext} in China, such as Beijing (46–54%) (Han et al., 2015), Chengdu (43%) (Tao et al., 2014),

260 Nanjing (53%) (Shen et al., 2014), and Xi'an (63%) (Cao et al., 2012), highlighting the dominant role of organic matters in aerosol light extinction in Xi'an today. Compared to the normal period, the contributions of NH$_4$NO$_3$, (NH$_4$)$_2$SO$_4$, fine soil, and BC, and POA to b_{ext} decreased by 1.3–7.6% in the lockdown, whereas contributions of two SOAs to b_{ext} increased by 3.0–14.6%. On the one hand, the mass concentrations of LO-OOA and MO-OOA decreased by 20.9–34.7%

from normal to lockdown periods, lower than those of other chemical species (35.8–72.5%); On the other hand, both of

265 SOAs MSEs and MAEs showed higher values during the lockdown period, especially MO-OOA. The combination of

effects eventually led to an enhanced role of SOA in light extinction during the lockdown.

3.4 Contribution of sources to b_{ext}

The six6-factor solution was selected to be the optimal solution, which can adequately account for the variability in

aerosolPM$_{2.5}$ concentration and optical coefficients b_{ext} (Figures S10 and S112). Six sources were determined by the

270 HERM analysis, consisting of traffic-related emission, biomass burning, coal combustion, fugitive dust, nitrate plus SOA

source, and sulfate plus SOA source. Details about their characteristics are presented in Figure 35. The first source

identified as traffic-related emission was characterized by high EV values of Cr (77%), Mn (53%), Fe (36%), and Zn

(39%), which can be released from lubricating oils, fuel additives, and brake and tire wear (Ålander et al., 2005;

Geivanidis et al., 2003; Tao et al., 2017; Zhang et al., 2013). Moderate contributions of POA (26%) and BC (28%) were

275 commonly regarded as species of diesel and gasoline engine exhaust (Chow et al., 2004; Liu et al., 2017). Additionally,

the temporal variations in b_{ext} from this source correlated well with NO$_x$ (R^2 = 0.72), suggesting an association with

motor vehicle emissions (Huang et al., 2017; Li et al., 2017a). The second source with high EV values of POA (45%),

LO-OOA (41%), BC (32%), Cl (34%), and K (41%) was judged to be biomass burning. K wasere regarded as an

excellent tracer of biomass burning (Li et al., 2007; Ni et al., 2017), and good correlations were also found between b_{ext}

280 from biomass burning and K (R^2 = 0.64). Previous studies have shown that POA from biomass burning can be rapidly

oxidized in the atmosphere (Cubison et al., 2011), therefore, the abundant LO-OOA observed in this source might be

indicative of aged biomass-burning aerosol (Crippa et al., 2013; Kim et al., 2017; Xu et al., 2015). The third source, coal

combustion, was characterized by high EV values of Cl (42%), As (38%), Se (46%), and Pb (25%). Of these elements,

As and Se had been found to bewere enriched in coals (Tian et al., 2013), which were reliable indicators for coal

285 combustion (Tan et al., 2017; Yu et al., 2019); and Pb was found to possibly emitted from coal combustion in Xi'an (Xu

et al., 2012). The fourth source was defined as fugitive dust due to significant EV values of Si (92%), Ca (63%), and Fe

(31%), which were the dominant chemical species in natural and construction dust profiles (Liu et al., 2017; Zhao et al.,

2006). Two secondary sources were resolved in our study as nitrate plus SOA source with high EV values of NO$_3^-$ (42%),

NH$_4^+$ (33%), and MO-OOA (34%) and sulfate plus SOA source with high EV values of SO$_4^{2-}$ (58%) and MO-OOA

290 (39%), respectively. Since SO$_2$ oxidation to sulfate needs a long time (e.g., 1 week) at the typical atmospheric level of

OH radicals, SO$_4^{2-}$ was likely associated with the regional source, while NO$_3^-$ was often formed more locally due to the

intense NO$_x$ emissions in China (Zhang et al., 2015; Zheng et al., 2014). The defined nitrate and sulfate plus SOA sources

appeared to have stronger associations with local and regional processes, respectively.

As shown in Figure 4̶6, the average b_{ext} from traffic-related emission, coal combustion and fugitive dust decreased from 77.3 $\pm$46.8 Mm^{-1}, 73.6 $\pm$60.9 Mm^{-1}, and 93.3 $\pm$82.7 Mm^{-1} during the normal period to 1.7 $\pm$4.0 Mm^{-1}, 38.5 $\pm$34.5 Mm^{-1}, and 30.8 $\pm$24.4 Mm^{-1} during the lockdown period, respectively, which can be explained by traffic restriction, closure of industries and stopping construction activities. b_{ext} from traffic-related emission with the largest reduction (97.9%) emphasized the effectiveness of controlling private gasoline cars and commercial and construction diesel trucks in the lockdown (Wang et al., 2020c). For two secondary sources, though previous studies reported the enhancement of secondary aerosol formation efficiencies as the increase of atmospheric oxidation capacity in the lockdown (Huang et al., 2020; Le et al., 2020; Tian et al., 2021), the decreases in gas and organic precursors (e.g., NO_2, SO_2, and VOCs) led to the 47.5% and 21.4% reductions of b_{ext} from sources of nitrate plus SOA and sulfate plus SOA, respectively. That is, the enhanced secondary aerosol cannot offset the primary emission reduction in Xi'an, confirming that reducing anthropogenic primary emissions is still the most effective treatment of aerosol pollution.

By contrast, the average b_{ext} from biomass burning during the lockdown period (215.4 $\pm$163.9 Mm^{-1}) was higher than that during the normal period (169.4 $\pm$196.9 Mm^{-1}). The government didn't strengthen the past control policies that forbade biomass burning in the lockdown. Moreover, strict controls were enforced on the movements of people, even in the countryside, possibly resulting more consumption of biomass for cooking and heating. As shown in Figure 5̶7, the rising stages of PM$_{2.5}$ during the lockdown period were all accompanied by the increase in b_{ext} from biomass burning, accounting for 46.4–55.6% of the total b_{ext}. Take the rising stage of PM$_{2.5}$ from 13:00 30 to 7:00 31 January as an example, b_{ext} from POA and LO-OOA increased rapidly at rates of 8.6 Mm^{-1} hour^{-1} and 8.2 Mm^{-1} hour^{-1}, respectively. Correspondingly, b_{ext} from biomass burning showed the fastest rise (26.0 Mm^{-1} hour^{-1}) in all primary source̲s, which̶t̶h̶a̶t led to biomass burning bec̲o̲m̲i̲n̲g̶a̶m̶e the most important source to b_{ext} (36.7%) in the lockdown (Figure 4̶6). Hence, additional actions and investigations on biomass burning emissions would be taken into consideration.

3.5 Impacts of COVID-19 lockdown on aerosol DRE

Figure 6̶ 8̲ shows the range of source-specific aerosol DRE$_{top}$, DRE$_{surface}$, and DRE$_{atmosphere}$ during the normal and lockdown periods. For all sources, the aerosol DRE$_{atmosphere}$ values in both periods were positive, producing net warming effects in the atmosphere. The mean aerosol DRE$_{atmosphere}$ decreased̶r̶e̶d̶u̶c̶e̶d from 31.0 $\pm$23.2 W m^{-2} before the lockdown to 14.1 $\pm$ 11.5 W m^{-2} in the lockdown, with a reduction of 54.5%̲.̲ ̲T̲h̲i̲s̲ ̲c̲a̲n̲ ̲b̲e̲ ̲e̲x̲p̲l̲a̲i̲n̲e̲d̲ ̲b̲y̲ ̲t̲h̲e̲ ̲r̲e̲d̲u̲c̲e̲d̲ ̲a̲e̲r̲o̲s̲o̲l̲ ̲c̲o̲n̲c̲e̲n̲t̲r̲a̲t̲i̲o̲n̲ ̲a̲n̲d̲ ̲i̲n̲c̲r̲e̲a̲s̲e̲d̲ ̲S̲S̲A̲ ̲(̲L̲i̲u̲ ̲e̲t̲ ̲a̲l̲.̲,̲ ̲2̲0̲2̲0̲)̲.

With regard to the contributions of specific sources on the DRE$_{atmosphere}$, traffic-related emission had the largest positive effect on DRE$_{atmosphere}$ during the normal period, with the value of 13.3 $\pm$9.2 W m^{-2}, followed by biomass burning (8.4 $\pm$13.0 W m^{-2}), coal combustion (7.8 $\pm$7.2 W m^{-2}), sulfate plus SOA source (1.7 $\pm$3.0 W m^{-2}), and fugitive dust (1.1 $\pm$

2.4 W m^{-2}). Nitrate and plus SOA source presented the negative value of DRE$_{atmosphere}$ (-1.2 $\pm$0.7 W m^{-2}), suggesting the

325 cooling effect in the atmosphere. Due to the strictest traffic restrictions implemented, the DRE$_{atmosphere}$ from traffic-related emission (0.4 $\pm$ 1.0 W m^{-2}) showed the a significant reduction (97.0%) in the lockdown. However, the DRE$_{atmosphere}$ from biomass burning increased to 10.0 $\pm$10.9 W m^{-2}, indicating that biomass burning was not effectively controlled during the lockdown period. The other four sources contributed relatively small amounts of DRE$_{atmosphere}$; that is 4.5 $\pm$4.5 W m^{-2} for coal combustion, -0.3 $\pm$0.8 W m^{-2} for fugitive dust, -1.4 $\pm$0.8 W m^{-2} for nitrate plus SOA source,

330 and 1.0 $\pm$ 1.8 W m^{-2} for sulfate plus SOA source. Similar to Xi'an city, the pollution sources of traffic and biomass burning were the two most significant anthropogenic sources of aerosol in most Chinese cities, such as Chengdu, Guangzhou, Jinan, Tianjin, and etc (Cheng et al., 2021; Huang et al., 2018; Khan et al., 2021; Li et al., 2017b). The results in this study indicated that the control measures on traffic in the lockdown were highly effective for mitigating the effects of climate change in the short -term, while future emission control policies should consider the importance of

335 biomass burning to tackle climate change in China.

4 Conclusion

This study conducted an intensive real-time measurement campaign in an urban city of China before and during the lockdown of Coronavirus Disease 2019 to investigate the impacts of anthropogenic emissions on aerosol optical properties and direct radiative effect (DRE). Decreases in light scattering coefficient (b_{scat}), light absorption coefficient

340 (b_{abs}), and light extinction coefficient (b_{ext}) were observed in the lockdown with reductions of 27.6–47.0%, in accord with the decline of PM$_{2.5}$ under strict emission control measures. Single scattering albedo during the lockdown period (0.92 $\pm$0.02) was higher than that during the normal period (0.89 $\pm$0.03), suggesting an enhanced role of secondary formation in the lockdown. The generalized addietive model analysis showed that meteorological conditions enhanced b_{ext} by 684.82 Mm^{-1} during the lockdown period, thus, the dramatical reduction of b_{ext} was totally credited to

345 anthropogenic emission reductions.

The relationship between b_{ext} and chemical components was established based on the ridge regression analysis. Using the estimated mass scattering and absorption efficiencies (MSEs and MAEs) of chemical components, OA including primary OA, less-, and more-oxidized oxygenated OA was found to be the largest contributor (45.1–61.4%) to b_{ext} before and during the lockdown period, followed by NH$_4$NO$_3$ (16.5–24.1%), BC (9.3–13.1%), (NH$_4$)$_2$SO$_4$ (7.9–11.2%), and

350 fine soil (4.9–6.5%). Particularly, secondary OA played an increasingly important part in light extinction during the lockdown when contributions of two oxygenated OAs to b_{ext} increased by 3.0–14.6%.

A hybrid environmental receptor model coupled with chemical and optical variables was utilized to carryied out optical source apportionment. Six sources of b_{ext} were resolved, including traffic-related emission, biomass burning, coal

combustion, fugitive dust, nitrate plus SOA source, and sulfate plus SOA source. Most ~~of~~ sources showed reductions of

355 b_{ext} (21.4–97.9%) during the lockdown, confirming the effectiveness of reducing anthropogenic primary emissions for treating aerosol pollution. b_{ext} from traffic-related emission had the most evident decrement (97.9%), whereas that from biomass burning increased by 27.1% during the lockdown due to the undiminished needs of residential cooking and heating in winter.

The atmospheric radiative transfer further illustrated that aerosol produced net warming effects (14.1–31.0 W m^{-2}) in the

360 atmosphere during the normal and lockdown periods. Biomass burning instead of traffic-related emission became the largest positive effect (10.0 ± 10.9 W m^{-2}) on aerosol DRE in the atmosphere in the lockdown. The results implied that reducing biomass burning would be another direct and effective way of~~n~~ climate change mitigation besides traffic restriction, therefore, the Chinese government should further tighten the policy on controlling biomass burning in the future.

References

380 Ålander, T., Antikainen, E., Raunemaa, T., Elonen, E., Rautiola, A., and Torkkell, K.: Particle emissions from a small two-stroke engine: Effects of fuel, lubricating oil, and exhaust aftertreatment on particle characteristics, Aerosol Sci. Tech., 39, 151–161, https://doi.org/1 0.1080/027868290910224, 2005.

Andreae, M. O. and Gelencsér, A.: Black carbon or brown carbon? The nature of light-absorbing carbonaceous aerosols, Atmos. Chem. Phys., 6, 3131–3148, https://doi.org/10.5194/acp-6-3131-2006, 2006.

385 Bellouin, N., Quaas, J., Morcrette, J. J., and Boucher, O.: Estimates of aerosol radiative forcing from the MACC re-analysis, Atmos. Chem. Phys., 13, 2045–2062, https://doi.org/10.5194/acp-13-2045-2013, 2013.

Cao, J. J., Wang, Q. Y., Chow, J. C., Watson, J. G., Tie, X. X., Shen, Z. X., Wang, P., and An, Z. S.: Impacts of aerosol compositions on visibility impairment in Xi'an, China, Atmos. Environ., 59, 559–566, https://doi.org/10.1016/j.atmosenv.2012.05.036, 2012.

390 Cappa, C. D., Che, D. L., Kessler, S. H., Kroll, J. H., and Wilson, K. R.: Variations in organic aerosol optical and hygroscopic properties upon heterogeneous OH oxidation, J. Geophys. Res.-Atmos., 116, D15204, https://doi.org/10.1029/2011JD015918, 2011.

Chamberlain-Ward, S. and Sharp, F.: Advances in Nephelometry through the Ecotech Aurora Nephelometer, The Scientific World Journal, 11, 2530–2535, https://doi.org/10.1100/2011/310769, 2011.

395 Chen, L. W. and Cao, J.: $PM_{2.5}$ source apportionment using a Hybrid Environmental Receptor Model, Environ. Sci. Technol., 52, 6357–6369, https://doi.org/10.1021/acs.est.8b00131, 2018.

Chen, Y., Zhang, S. M., Peng, C., Shi, G. M., Tian, M., Huang, R. J., Guo, D. M., Wang, H. B., Yao, X. J., and Yang, F. M.: Impact of the COVID-19 pandemic and control measures on air quality and aerosol light absorption in southwestern China, Sci. Total Environ., 749, 141419, https://doi.org/10.1016/j.scitotenv.2020.141419, 2020.

400 Cheng, M. T., Tang, G. Q., Lv, B., Li, X. R., Wu, X. R., Wang, Y. M., and Wang, Y. S.: Source apportionment of $PM_{2.5}$ and visibility in Jinan, China, J. Environ. Sci., 102, 207–215, https://doi.org/10.1016/j.jes.2020.09.012, 2021.

Cheng, Z., Jiang, J. K., Chen, C. H., Gao, J., Wang, S. X., Watson, J. G., Wang, H. L., Deng, J. G., Wang, B. Y., Zhou, M., Chow, J. C., Pitchford, M. L., and Hao, J. M.: Estimation of aerosol mass scattering efficiencies under high mass loading: Case study for the megacity of Shanghai, China, Environ. Sci. Technol., 49, 831–838, 405 https://doi.org/10.1021/es504567q, 2015.

China National Environmental Monitoring Centre (CNEMC).: Background values of soil elements in China, Chinese Environmental Press, Beijing (in Chinese), 1990.

Chow, J. C., Lowenthal, D. H., Chen, L. W. A., Wang, X. L., and Watson, J. G.: Mass reconstruction methods for $PM_{2.5}$: a review, Air Qual. Atmos. Health, 8, 243–263, https://doi.org/10.1007/s11869-015-0338-3, 2015.

410 Chow, J. C., Watson, J. G., Kuhns, H., Etyemezian, V., Lowenthal, D. H., Crow, D., Kohl, S. D., Engelbrecht, J. P., and Green, M. C.: Source profiles for industrial, mobile, and area sources in the Big Bend Regional Aerosol Visibility and Observational study, Chemosphere, 54, 185–208, https://doi.org/10.1016/j.chemosphere.2003.07.004, 2004.

Crippa, M., DeCarlo, P. F., Slowik, J. G., Mohr, C., Heringa, M. F., Chirico, R., Poulain, L., Freutel, F., Sciare, J., Cozic, J., Di Marco, C. F., Elsasser, M., Nicolas, J. B., Marchand, N., Abidi, E., Wiedensohler, A., Drewnick, F., Schneider, 415 J., Borrmann, S., Nemitz, E., Zimmermann, R., Jaffrezo, J. L., Prévôt, A. S. H., and Baltensperger, U.: Wintertime aerosol chemical composition and source apportionment of the organic fraction in the metropolitan area of Paris, Atmos. Chem. Phys., 13, 961–981, https://doi.org/10.5194/acp-13-961-2013, 2013.

Cubison, M. J., Ortega, A. M., Hayes, P. L., Farmer, D. K., Day, D., Lechner, M. J., Brune, W. H., Apel, E., Diskin, G. S., Fisher, J. A., Hecobian, A., Knapp, D. J., Mikoviny, T., Riemer, D., Sachse, G. W., Sessions, W., Weber, R. J., 420 Weinheimer, A. J., and Jimenez, J. L.: Effects of aging on organic aerosol from open biomass burning smoke in aircraft and lab studies, Atmos. Chem. Phys., 11, 12049–12064, https://doi.org/10.5194/acpd-11-12103-2011, 2011.

Deng, J. J., Zhang, Y. R., Hong, Y. W., Xu, L. L., Chen, Y. T., Du, W. J., and Chen, J. S.: Optical properties of $PM_{2.5}$ and the impacts of chemical compositions in the coastal city Xiamen in China, Sci. Total Environ., 557–558, 665–675, https://doi.org/10.1016/j.scitotenv.2016.03.143, 2016.

425 Drinovec, L., Močnik, G., Zotter, P., Prévôt, A. S. H., Ruckstuhl, C., Coz, E., Rupakheti, M., Sciare, J., Müller, T., Wiedensohler, A., and Hansen, A. D. A.: The "dual-spot" Aethalometer: an improved measurement of aerosol black

carbon with real-time loading compensation, Atmos. Meas. Tech., 8, 1965–1979, https://doi.org/10.5194/amt-8-1965-2015, 2015.

Feng, Y., Ramanathan, V., and Kotamarthi, V. R.: Brown carbon: a significant atmospheric absorber of solar radiation? Atmos. Chem. Phys., 13, 8607–8621, https://doi.org/10.5194/acp-13-8607-2013, 2013.

Flores, J. M., Zhao, D. F., Segev, L., Schlag, P., Kiendler-Scharr, A., Fuchs, H., Watne, A. K., Bluvshtein, N., Mentel, T. F., and Hallquist, M.: Evolution of the complex refractive index in the UV spectral region in ageing secondary organic aerosol, Atmos. Chem. Phys., 14, 5793–5806, https://doi.org/10.5194/acp-14-5793-2014, 2014.

Forello, A. C., Bernardoni, V., Calzolai, G., Lucarelli, F., Massabò, D., Nava, S., Pileci, R. E., Prati, P., Valentini, S., Valli, G., and Vecchi, R.: Exploiting multi-wavelength aerosol absorption coefficients in a multi-time resolution source apportionment study to retrieve source-dependent absorption parameters, Atmos. Chem. Phys., 19, 11235–11252, https://doi.org/10.5194/acp-19-11235-2019, 2019.

Furger, M., Rai, P., Slowik, J. G., Cao, J. J., Visser, S., Baltensperger, U., and Prévôt, A. S. H.: Automated alternating sampling of PM_{10} and $PM_{2.5}$ with an online XRF spectrometer, Atmos. Environ.: X, 5, 100065, https://doi.org/10.1016/j.aeaoa.2020.100065, 2020.

Geivanidis, S., Pistikopoulos, P., and Samaras, Z.: Effect on exhaust emissions by the use of methylcyclopentadienyl manganese tricarbonyl (MMT) fuel additive and other lead replacement gasolines, Sci. Total Environ., 305, 129–141, https://doi.org/10.1016/S0048-9697(02)00476-X, 2003.

Hallquist, M., Wenger, J. C., Baltensperger, U., Rudich, Y., Simpson, D., Claeys, M., Dommen, J., Donahue, N. M., George, C., Goldstein, A. H., Hamilton, J. F., Herrmann, H., Hoffmann, T., Iinuma, Y., Jang, M., Jenkin, M. E., Jimenez, J. L., Kiendler-Scharr, A., Maenhaut, W., McFiggans, G., Mentel, Th. F., Monod, A., Prévôt, A. S. H., Seinfeld, J. H., Surratt, J. D., Szmigielski, R., and Wildt, J.: The formation, properties and impact of secondary organic aerosol: current and emerging issues, Atmos. Chem. Phys., 9, 5155–5236, https://doi.org/10.5194/acp-9-5155-2009, 2009.

Han, T. T., Xu, W. Q., Chen, C., Liu, X. G., Wang, Q. Q., Li, J., Zhao, X. J., Du, W., Wang, Z. F., and Sun, Y. L.: Chemical apportionment of aerosol optical properties during the Asia-Pacific Economic Cooperation summit in Beijing, China, J. Geophys. Res.-Atmos., 120, 12281–12295, https://doi.org/10.1002/2015JD023918, 2015.

Herich, H., Hueglin, C., and Buchmann, B.: A 2.5 year's source apportionment study of black carbon from wood burning and fossil fuel combustion at urban and rural sites in Switzerland, Atmos. Meas. Tech., 4, 1409–1420, https://doi.org/10.5194/amt-4-1409-2011, 2011.

Hess, M., Koepke, P., and Schult, I.: Optical properties of aerosols and clouds: The software package OPAC, B. Am. Meteorol. Soc., 79, 831–844, https://doi.org/10.1175/1520-0477(1998)079<0831:OPOAAC>2.0.CO;2, 1998.

Huang, X., Ding, A. J., Gao, J., Zheng, B., Zhou, D. R., Qi, X. M., Tang, R., Wang, J. P., Ren, C. H., Nie, W., Chi, X. G., Xu, Z., Chen, L. D., Li, Y. Y., Che, F., Pang, N. N., Wang, H. K., Tong, D., Qin, W., Cheng, W., Liu, W. J., Fu, Q. Y., Liu, B. X., Chai, F., Davis, J. S., Zhang, Q., and He, K. B.: Enhanced secondary pollution offset reduction of primary emissions during COVID-19 lockdown in China, Natl. Sci. Rev., 8, nwaa137, https://doi.org/10.1093/nsr/nwaa137, 2020.

Huang, X. F., Zou, B. B., He, L. Y., Hu, M., Prévôt, A. S. H., and Zhang, Y. H.: Exploration of $PM_{2.5}$ sources on the regional scale in the Pearl River Delta based on ME-2 modeling, Atmos. Chem. Phys., 18, 11563–11580, https://doi.org/10.5194/acp-18-11563-2018, 2018.

Huang, X. J., Liu, Z. R., Liu, J. Y., Hu, B., Wen, T. X., Tang, G. Q., Zhang, J. K., Wu, F. K., Ji, D. S., Wang, L. L., and Wang, Y. S.: Chemical characterization and source identification of $PM_{2.5}$ at multiple sites in the Beijing-Tianjin-Hebei region, China, Atmos. Chem. Phys., 17, 12941–12962, https://doi.org/10.5194/acp-17-12941-2017, 2017.

470 Ibrahim, S., Landa, M., Pešek, O., Pavelka, K., and Halounova, L.: Space-time machine learning models to analyze COVID-19 pandemic lockdown effects on aerosol optical depth over Europe, Remote Sens., 13, 3027, https://doi.org/10.3390/rs13153027, 2021.

IPCC: Climate change 2013: The physical science basis. Contribution of working group I to the fifth assessment reprot of the intergovemental panel on climate change [Stocker, T. F., D. Qin, G. -K. Plattner, M. Tignor, S. K. Allen, J.
475 Boschung, A. Nauels, Y. Xia, V. Bex and P.M. Midgley (eds.)]. Cambridge University Press, Cambrigde, United Kingdom and New York, NY, USA, 1535pp, 2013.

Khan, J. Z., Sun, L., Tian, Y. Z., Shi, G. L., and Feng, Y. C.: Chemical characterization and source apportionment of PM_1 and $PM_{2.5}$ in Tianjin, China: Impacts of biomass burning and primary biogenic sources, J. Environ. Sci., 99, 196–209, https://doi.org/10.1016/j.jes.2020.06.027, 2021.

480

Kim, H., Zhang, Q., Bae, G. N., Kim, J. Y., and Lee, S. B.: Sources and atmospheric processing of winter aerosols in Seoul, Korea: Insights from real-Time measurements using a high-resolution aerosol mass spectrometer, Atmos. Chem. Phys., 17, 2009–2033, https://doi.org/10.5194/acp-17-2009-2017, 2017.

Kirchstetter, T.W., Novakov, T., and Hobbs, P. V.: Evidence that the spectral dependence of light absorption by aerosols
485 is affected by organic carbon, J. Geophys. Res.-Atmos., 109, D21208, doi:10.1029/2004JD004999, 2004.

Kumar, D., Singh, A. K., Kumar, V., Poyoja, R., Ghosh, A., and Singh, B.: COVID-19 driven changes in the air quality; a study of major cities in the Indian state of Uttar Pradesh, Environ. Pollut., 274, 116512, https://doi.org/10.1016/j.envpol.2021.116512, 2021.

Laskin, A., Laskin, J., and Nizkorodov, S. A.: Chemistry of atmospheric brown carbon, Chem. Rev., 115, 10, 4335–
490 4382, https://doi.org/10.1021/cr5006167, 2015.

Le, T. H., Wang, Y., Liu, L., Yang, J. N., Yung, Y., Li, G. H., and Seinfeld, J. H.: Unexpected air pollution with marked emission reductions during the COVID-19 outbreak in China, Science, 369, 702–706, https://doi.org/10.1126/science.abb7431, 2020.

Lee, H. J., Aiona, P. K., Laskin, A., Laskin, J., and Nizkorodov, S. A.: Effect of solar radiation on the optical properties
495 and molecular composition of laboratory proxies of atmospheric brown carbon, Environ. Sci. Technol., 48, 10217–10226, https://doi.org/10.1021/es502515r, 2014.

Li, H. Y., Zhang, Q., Zhang, Q., Chen, C. R., Wang, L. T., Wei, Z., Zhou, S., Parworth, C., Zheng, B., Canonaco, F., Prévôt, A. S. H., Chen, P., Zhang, H. L., Wallington, T. J., and He, K. B.: Wintertime aerosol chemistry and haze evolution in an extremely polluted city of the North China Plain: significant contribution from coal and biomass
500 combustion, Atmos. Chem. Phys., 17, 4751–4768, https://doi.org/10.5194/acp-17-4751-2017, 2017a.

Li, L., Li, Q., Huang, L., Wang, Q., Zhu, A. S., Xu, J., Liu, Z. Y., Li, H. L., Shi, L. S., Li, R., Azari, M., Wang, Y. J., Zhang, X. J., Liu, Z. Q., Zhu, Y. H., Zhang, K., Xue, S. H., Ooi, M. C. G., Zhang, D. P., and Chan, A.: Air quality changes during the COVID-19 lockdown over the Yangtze River Delta Region: An insight into the impact of human activity pattern changes on air pollution variation, Sci. Total Environ., 732, 139282,
505 https://doi.org/10.1016/j.scitotenv.2020.139282, 2020.

Li, L. L, Tan, Q. W., Zhang, Y. H., Feng, M., Qu, Y., An, J. L., and Liu, X. G.: Characteristics and source apportionment of $PM_{2.5}$ during persistent extreme haze events in Chengdu, southwest China, Environ. Pollut., 230, 718–729, https://doi.org/10.1016/j.envpol.2017.07.029, 2017b.

Li, X. H., Wang, S. X., Duan, L., Hao, J. M., Li, C., Chen, Y. S., and Yang, L.: Particulate and trace gas emissions from open burning of wheat straw and corn stover in China, Environ. Sci. Technol., 41, 6052–6058, https://doi.org/10.1021/es0705137, 2007.

Lin, G. X., Penner, J. E., Flanner, M. G., Sillman, S., Xu, L., and Zhou, C.: Radiative forcing of organic aerosol in the atmosphere and on snow: Effects of SOA and brown carbon, J. Geophys. Res.-Atmos., 119, 7453–7476, https://doi.org/10.1002/2013JD021186, 2014.

Lin, Y. C., Zhang, Y. L., Xie, F., Fan, M. Y., and Liu, X.: Substantial decreases of light absorption, concentrations and relative contributions of fossil fuel to light-absorbing carbonaceous aerosols attributed to the COVID-19 lockdown in east China, Environ. Pollut., 275, 116615, https://doi.org/10.1016/j.envpol.2021.116615, 2021.

Liu, B. S., Wu, J. H., Zhang, J. Y., Wang, L., Yang, J. M., Liang, D. N., Dai, Q. L., Bi, X. H., Feng, Y. C., Zhang, Y. F., and Zhang, Q. X.: Characterization and source apportionment of PM$_{2.5}$ based on error estimation from EPA PMF 5.0 model at a medium city in China, Environ. Pollut., 222, 10–22, https://doi.org/10.1016/j.envpol.2017.01.005, 2017.

Liu, D. T., Hu, K., Zhao, D. L., Ding, S., Wu, Y. F., Zhou, C., Yu, C. J., Tian, P., Liu, Q., Bi, K., Wu, Y. Z., Hu, B., Ji, D. S., Kong, S. F., Ouyang, B., He, H., Huang, M. Y., and Ding, D. P.: Efficient vertical transport of black carbon in the planetary boundary layer, Geophys. Res. Lett., 47, e2020GL088858, https://doi.org/10.1029/2020GL088858, 2020.

Ma, X., Yu, F., and Luo, G.: Aerosol direct radiative forcing based on GEOS-Chem-APM and uncertainties, Atmos. Chem. Phys., 12, 5563–5581, https://doi.org/10.5194/acp-12-5563-2012, 2012.

Malm, W. C. and Hand, J. L.: An examination of the physical and optical properties of aerosols collected in the IMPROVE program, Atmos. Environ., 41, 3407–3427, https://doi.org/10.1016/j.atmosenv.2006.12.012, 2007.

Moise, T., Flores, J. M., and Rudich, Y.: Optical properties of secondary organic aerosols and their changes by chemical processes, Chem. Rev., 115, 4400–4439, https://doi.org/10.1021/cr5005259, 2015.

Ng, N. L., Herndon, S. C., Trimborn, A., Canagaratna, M. R., Croteau, P. L., Onasch, T. B., Sueper, D., Worsnop, D. R., Zhang, Q., Sun, Y. L., and Jayne, J. T.: An aerosol chemical speciation monitor (ACSM) for routine monitoring of the composition and mass concentrations of ambient aerosol, Aerosol Sci. Technol., 45, 780–794, https://doi.org/10.1080/02786826.2011.560211, 2011.

Ni, H. Y., Tian, J., Wang, X. L., Wang, Q. Y., Han, Y. M., Cao, J. J., Long, X., Chen, L.-W. A., Chow, J. C., and Watson, J. G.: PM$_{2.5}$ emissions and source profiles from open burning of crop residues, Atmos. Environ., 169, 229–237, https://doi.org/10.1016/j.atmosenv.2017.08.063, 2017.

Niu, X. Y., Cao, J. J., Shen, Z. X., Ho, S. S. H., Tie, X. X., Zhao, S. Y., Xu, H. M., Zhang, T., and Huang, R. J.: PM$_{2.5}$ from the Guanzhong Plain: Chemical composition and implications for emission reductions, Atmos. Environ., 147, 458–469, https://doi.org/10.1016/j.atmosenv.2016.10.029, 2016.

Norris, G., Duvall, R., Brown, S., and Bai, S.: EPA positive matrix factorization (PMF) 5.0 fundamentals and user guide, 2014.

Qin, Y. M., Tan, H. B., Li, Y. J., Li, Z. J., Schurman, M. I., Liu, L., Wu, C., and Chan, C. K.: Chemical characteristics of brown carbon in atmospheric particles at a suburban site near Guangzhou, China, Atmos. Chem. Phys., 18, 16409–16418, https://doi.org/10.5194/acp-18-16409-2018, 2018.

Rai, P., Furger, M., Slowik, J. G., Canonaco, F., Fröhlich, R., Hüglin, C., Minguillón, M. C., Petterson, K., Baltensperger, U., and Prévôt, A. S. H.: Source apportionment of highly time-resolved elements during a firework episode from a rural freeway site in Switzerland, Atmos. Chem. Phys., 20, 1657–1674, https://doi.org/10.5194/acp-20-1657-2020, 2020.

Ricchiazzi, P., Yang, S. R., Gautier, C., and Sowle, D.: SBDART: A research and teaching software tool for Plane-parallel radiative transfer in the Earth's atmosphere, B. Am. Meteorol. Soc., 79, 2101–2114, https://doi.org/10.1175/1520-0477(1998)079<2101:SARATS>2.0.CO;2, 1998.

555 Saarikoski, S., Niemi, J. V., Aurela, M., Pirjola, L., Kousa, A., Rönkkö, T., and Timonen, H.: Sources of black carbon at residential and traffic environments obtained by two source apportionment methods, Atmos. Chem. Phys., 21, 14851–14869, https://doi.org/10.5194/acp-21-14851-2021, 2021.

Sanap, S. D.: Global and regional variations in aerosol loading during COVID-19 imposed lockdown, Atmos. Environ., 246, 118132, https://doi.org/10.1016/j.atmosenv.2020.118132, 2021.

Sandradewi, J., Prévôt, A. S. H., Szidat, S., Perron, N., Alfarra, M. R., Lanz, V. A., Weingartner, E., and Baltensperger,
560 U.: Using aerosol light absorption measurements for the quantitative determination of wood burning and traffic emission contributions to particulate matter, Environ. Sci. Technol., 42, 3316–3323, https://doi.org/10.1021/es702253m, 2008.

Schimek, M. G.: Semiparametric penalized generalized additive models for environmental research and epidemiology, Environmetrics, 20, 699–717, https://doi.org/10.1002/env.972, 2009.

565 Shen, G. F., Xue, M., Yuan, S. Y., Zhang, J., Zhao, Q. Y., Li, B., Wu, H. S., and Ding, A. J.: Chemical compositions and reconstructed light extinction coefficients of particulate matter in a mega-city in the western Yangtze River Delta, China, Atmos. Environ., 83, 14–20, https://doi.org/10.1016/j.atmosenv.2013.10.055, 2014.

Tan, J. H., Zhang, L. M., Zhou, X. M., Duan, J. C., Li, Y., Hu, J. N., and He, K. B.: Chemical characteristics and source apportionment of $PM_{2.5}$ in Lanzhou, China, Sci. Total Environ., 601–602, 1743–1752,
570 https://doi.org/10.1016/j.scitotenv.2017.06.050, 2017.

Tao, J., Zhang, L. M., Cao, J. J., Zhong, L. J., Chen, D. S., Yang, Y. H., Chen, D. H., Chen, L. G., Zhang, Z. S., Wu, Y., Xia, Y. J., Ye, S. Q., and Zhang, R. J.: Source apportionment of $PM_{2.5}$ at urban and suburban areas of the Pearl River Delta region, south China - With emphasis on ship emissions, Sci. Total Environ., 574, 1559–1570, https://doi.org/10.1016/j.scitotenv.2016.08.175, 2017.

575 Tao, J., Zhang, L. M., Cao, J., Hsu, S. C., Xia, X. G., Zhang, Z. S., Lin, Z. J., Cheng, T. T., and Zhang, R. J.: Characterization and source apportionment of aerosol light extinction in Chengdu, southwest China, Atmos. Environ., 95, 552–562, https://doi.org/10.1016/j.atmosenv.2014.07.017, 2014.

Tao, J., Zhang, L. M., Gao, J., Wang, H., Chai, F. H., and Wang, S. L: Aerosol chemical composition and light scattering during a winter season in Beijing, Atmos. Environ., 110, 36–44, https://doi.org/10.1016/j.atmosenv.2015.03.037,
580 2015.

Tian, H. Z., Lu, L., Hao, J. M., Gao, J. J., Cheng, K., Liu, K. Y., Qiu, P. P., and Zhu, C. Y.: A review of key hazardous trace elements in Chinese coals: Abundance, occurrence, behavior during coal combustion and their environmental impacts, Energ. Fuel., 27, 601–614, https://doi.org/10.1021/ef3017305, 2013.

Tian, J., Wang, Q. Y., Han, Y. M., Ye, J. H., Wang, P., Pongpiachan, S., Ni, H. Y., Zhou, Y. Q., Wang, M., Zhao, Y. Z.,
585 and Cao, J. J.: Contributions of aerosol composition and sources to particulate optical properties in a southern coastal city of China, Atmos. Res., 235, 104744, https://doi.org/ 10.1016/j.atmosres.2019.104744, 2020.

Tian, J., Wang, Q. Y., Ni, H. Y., Wang, M., Zhou, Y. Q., Han, Y. M., Shen, Z. X., Pongpiachan, S., Zhang, N. N., Zhao, Z. Z., Zhang, Q., Zhang, Y., Long, X., and Cao, J. J.: Emission characteristics of primary brown carbon absorption from biomass and coal burning: Development of an optical emission inventory for China, J. Geophys. Res.-Atmos.,
590 124, 1879–1893, https://doi.org/10.1029/2018JD029352, 2019.

Tian, J., Wang, Q. Y., Zhang, Y., Yan, M. Y., Liu, H. K., Zhang, N. N., Ran, W. K., and Cao, J. J.: Impacts of primary emissions and secondary aerosol formation on air pollution in an urban area of China during the COVID-19 lockdown, Environ. Int., 150, 106426, https://doi.org/10.1016/j.envint.2021.106426, 2021.

595 Ulbrich, I. M., Canagaratna, M. R., Zhang, Q., Worsnop, D. R., and Jimenez, J. L.: Interpretation of organic components from Positive Matrix Factorization of aerosol mass spectrometric data, Atmos. Chem. Phys., 9, 2891–2918, https://doi.org/10.5194/acp-9-2891-2009, 2009.

Wang, J. F., Ye, J. H., Zhang, Q., Zhao, J., Wu, Y. Z., Li, J. Y., Liu, D. T., Li, W. J., Zhang, Y. G., Wu, C., Xie, C. H., Qin, Y. M., Lei, Y. L., Huang, X. P., Guo, J. P., Liu, P. F., Fu, P. Q., Li, Y. J., Lee, H. C., Choi, H., Zhang, J., Liao, H., Chen, M. D., Sun, Y. L., Ge, X. L., Martin, S. T., and Jacob, D. J.: Aqueous production of secondary organic
600 aerosol from fossil-fuel emissions in winter Beijing haze, P. Natl. Acad. Sci. USA., 118, e2022179118, https://doi.org/10.1073/pnas.2022179118, 2021.

Wang, P., Cao, J. J., Shen, Z. X., Han, Y. M., Lee, S. C., Huang, Y., Zhu, C. S., Wang, Q. Y., Xu, H. M., and Huang, R. J.: Spatial and seasonal variations of $PM_{2.5}$ mass and species during 2010 in Xi'an, China, Sci. Total Environ., 508, 477–487, https://doi.org/10.1016/j.scitotenv.2014.11.007, 2015.

605 Wang, P.F., Chen, K.Y., Zhu, S.Q., Wang, P., and Zhang, H.L.: Severe air pollution events not avoided by reduced anthropogenic activities during COVID-19 outbreak, Resour. Conserv. Recycl., 158, 104814, https://doi.org/10.1016/j.resconrec.2020.104814, 2020a.

Wang, Q. Y., Liu, H. K., Wang, P., Dai, W. T., Zhang, T., Zhao, Y. Z., Tian, J., Zhang, W. Y., Han, Y. M., and Cao, J. J.: Optical source apportionment and radiative effect of light-absorbing carbonaceous aerosols in a tropical marine
610 monsoon climate zone: the importance of ship emissions, Atmos. Chem. Phys., 20, 15537–15549, https://doi.org/10.5194/acp-20-15537-2020, 2020b.

Wang, X., Heald, C. L., Ridley, D. A., Schwarz, J. P., Spackman, J. R., Perring, A. E., Coe, H., Liu, D., and Clarke, A. D.: Exploiting simultaneous observational constraints on mass and absorption to estimate the global direct radiative forcing of black carbon and brown carbon, Atmos. Chem. Phys., 14, 17527–17583, https://doi.org/10.5194/acp-14-
615 10989-2014, 2014.

Wang, Y. C., Yuan, Y., Wang, Q. Y., Liu, C. G., Zhi, Q., and Cao, J. J.: Changes in air quality related to the control of coronavirus in China: Implications for traffic and industrial emissions, Sci. Total Environ., 731, 139133, https://doi.org/10.1016/j.scitotenv.2020.139133, 2020c.

Weber, J., Shin, Y. M., Staunton Sykes, J., Archer-Nicholls, S., Abraham, N. L., and Archibald, A. T.: Minimal climate
620 impacts from short-lived climate forcers following emission reductions related to the COVID-19 pandemic, Geophys. Res. Lett., 47, e2020GL090326. https://doi.org/10.1029/2020GL090326, 2020.

Wood, S. N.: Generalized additive models: An introduction with R (2nd ed), CRC press, 496pp, https://doi.org/10.1201/9781315370279, 2017.

Wood, S. N.: Stable and efficient multiple smoothing parameter estimation for generalized additive models, J. Am. Stat.
625 Assoc., 99, 673–686, https://doi.org/10.1198/016214504000000980, 2004.

Wu, J. R., Bei, N. F., Li, X., Cao, J. J., Feng, T., Wang, Y. C., Tie, X. X., and Li, G. H.: Widespread air pollutants of the North China Plain during the Asian summer monsoon season: a case study, Atmos. Chem. Phys., 18, 8491–8504, https://doi.org/10.5194/acp-18-8491-2018, 2018.

Xie, M. J., Chen, X., Holder, A. L., Hays, M. D., Lewandowski, M., Offenberg, J. H., Kleindienst, T. E., Jaoui, M., and
630 Hannigan, M. P.: Light absorption of organic carbon and its sources at a southeastern U.S. location in summer, Environ. Pollut., 244, 38–46, https://doi.org/10.1016/j.envpol.2018.09.125, 2019.

Xu, H. M., Cao, J. J., Ho, K. F., Ding, H., Han, Y. M., Wang, G. H., Chow, J. C., Watson, J. G., Khol, S. D., Qiang, J., Li, W. T.: Lead concentrations in fine particulate matter after the phasing out of leaded gasoline in Xi'an, China, Atmos. Environ., 46, 217–224, https://doi.org/10.1016/j.atmosenv.2011.09.078, 2012.

635 Xu, L., Zhang, J., Sun, X., Xu, S. C., Shan, M., Yuan, Q., Liu, L., Du, Z. H., Liu, D. T., Xu, D., Song, C. B., Liu, B. W., Lu, G. D., Shi, Z. B., and Li, W. J.: Variation in concentration and sources of black carbon in a megacity of China during the COVID-19 pandemic, Geophys. Res. Lett., 47, e2020GL090444, https://doi.org/10.1029/2020GL090444, 2020a.

Xu, W. Q., Sun, Y. L., Chen, C., Du, W., Han, T. T., Wang, Q. Q., Fu, P. Q., Wang, Z. F., Zhao, X. J., Zhou, L. B., Ji, 640 D. S., Wang, P. C., and Worsnop, D. R.: Aerosol composition, oxidation properties, and sources in Beijing: results from the 2014 Asia-Pacific Economic Cooperation summit study, Atmos. Chem. Phys., 15, 13681–13698, https://doi.org/10.5194/acp-15-13681-2015, 2015.

Xu, W. Y., Kuang, Y., Bian, Y. X., Liu, L., Li, F., Wang, Y. Q., Xue, B., Luo, B., Huang, S., Yuan, B., Zhao, P. S., and Shao, M.: Current challenges in visibility improvement in southern China, Environ. Sci. Technol. Lett., 7, 395–401, 645 https://doi.org/10.1021/acs.estlett.0c00274, 2020b.

Yao, H., Song, Y., Liu, M. X., Archer-Nicholls, S., Lowe, D., McFiggans, G., Xu, T. T., Du, P., Li, J. F., Wu, Y. S., Hu, M., Zhao, C., and Zhu, T.: Direct radiative effect of carbonaceous aerosols from crop residue burning during the summer harvest season in East China, Atmos. Chem. Phys., 17, 5205–5219, https://doi.org/10.5194/acp-17-5205-2017, 2017.

650 Yao, L. Q., Kong, S. F., Zheng, H., Chen, N., Zhu, B., Xu, K., Cao, W. X., Zhang, Y., Zheng, M. M., Cheng, Y., Hu, Y., Zhang, Z. X., Yan, Y. Y., Liu, D. T., Zhao, T. L., Bai, Y. Q., and Qi, S. H.: Co-benefits of reducing $PM_{2.5}$ and improving visibility by COVID-19 lockdown in Wuhan, NPJ Clim. Atmos. Sci., 4, 40, https://doi.org/ 10.1038/s41612-021-00195-6, 2021.

Yao, M. S., Zhang, L., Ma, J. X., and Zhou, L.: On airborne transmission and control of SARS-Cov-2, Sci. Total Environ., 655 731, 139178, https://doi.org/10.1016/j.scitotenv.2020.139178, 2020.

Yu, Y. Y., He, S. Y., Wu, X. L., Zhang, C., Yao, Y., Liao, H., Wang, Q. G., and Xie, M. J.: $PM_{2.5}$ elements at an urban site in Yangtze River Delta, China: High time-resolved measurement and the application in source apportionment, Environ. Pollut., 253, 1089–1099, https://doi.org/10.1016/j.envpol.2019.07.096, 2019.

Zhang, R., Jing, J., Tao, J., Hsu, S. C., Wang, G., Cao, J., Lee, C. S. L., Zhu, L., Chen, Z., Zhao, Y., and Shen, Z.: 660 Chemical characterization and source apportionment of $PM_{2.5}$ in Beijing: seasonal perspective, Atmos. Chem. Phys., 13, 7053–7074, https://doi.org/10.5194/acp-13-7053-2013, 2013.

Zhang, R. Y., Wang, G. H., Guo, S., Zamora, M. L., Ying, Q., Lin, Y., Wang, W. G., Hu, M., and Wang, Y.: Formation of urban fine particulate matter, Chem. Rev., 115, 3803–3855, https://doi.org/10.1021/acs.chemrev.5b00067, 2015.

Zhang, Q., Shen, Z. X., Zhang, L. M., Zeng, Y. L., Ning, Z., Zhang, T., Lei, Y. L., Wang, Q. Y., Li, G. H., Sun, J., 665 Westerdahl, D., Xu, H. M., and Cao, J. J.: Investigation of primary and secondary particulate brown carbon in two Chinese cities of Xi'an and Hong Kong in wintertime, Environ. Sci. Technol., 54, 3803 – 3813, https://doi.org/10.1021/acs.est.9b05332, 2020.

Zhao, P. S., Feng, Y. C., Tan, Z., and Wu, J. H.: Characterizations of resuspended dust in six cities of North China, Atmos. Environ., 40, 5807–5814, https://doi.org/10.1016/j.atmosenv.2006.05.026, 2006.

670 Zhao, Y. B., Zhang, K., Xu, X. T., Shen, H. Z., Zhu, X., Zhang, Y. X., Hu, Y. T., and Shen, G. F.: Substantial changes in nitrogen dioxide and ozone after excluding meteorological impacts during the COVID-19 outbreak in mainland China, Environ. Sci. Technol. Lett., 7, 402–408, https://doi.org/10.1021/acs.estlett.0c00304, 2020.

Zheng, B., Huo, H., Zhang, Q., Yao, Z. L., Wang, X. T., Yang, X. F., Liu, H., and He, K. B.: High-resolution mapping of vehicle emissions in China in 2008, Atmos. Chem. Phys., 14, 9787–9805, https://doi.org/10.5194/acp-14-9787-2014, 2014.

Zheng, B., Tong, D., Li, M., Liu, F., Hong, C. P., Geng, G. N., Li, H. Y., Li, X., Peng, L. Q., Qi, J., Yan, L., Zhang, Y. X., Zhao, H. Y., Zheng, Y. X., He, K. B., and Zhang, Q.: Trends in China's anthropogenic emissions since 2010 as the consequence of clean air actions, Atmos. Chem. Phys., 18, 14095–14111, https://doi.org/10.5194/acp-18-14095-2018, 2018.

Zheng, H., Kong, S. F., Chen, N., Yan, Y. Y., Liu, D. T., Zhu, B., Xu, K., Cao, W. X., Ding, Q. Q., Lan, B., Zhang, Z. X., Zheng, M. M., Fan, Z. W., Cheng, Y., Zheng, S. R., Yao, L. Q., Bai, Y. Q., Zhao, T. L., and Qi, S. H.: Significant changes in the chemical compositions and sources of $PM_{2.5}$ in Wuhan since the city lockdown as COVID-19. Sci. Total Environ., 739, 140000, https://doi.org/10.1016/j.scitotenv.2020.140000, 2020.

Zhou, Y. Q., Wang, Q. Y., Huang, R. J., Liu, S. X., Tie, X. X., Su, X. L., Niu, X. Y., Zhao, Z. Z., Ni, H. Y., Wang, M., Zhang, Y. G., and Cao, J. J.: Optical properties of aerosols and implications for radiative effects in Beijing during the Asia-Pacific Economic Cooperation (APEC) Summit 2014, J. Geophys. Res.-Atmos., 122, 10119–10132, https://doi.org/10.1002/2017jd026997, 2017.

Zotter, P., Herich, H., Gysel, M., El-Haddad, I., Zhang, Y., Močnik, G., Hüglin, C. Baltensperger, U., Szidat, S., and Prévôt, A. S. H.: Evaluation of the absorption Ångström exponents for traffic and wood burning in the Aethalometer-based source apportionment using radiocarbon measurements of ambient aerosol, Atmos. Chem. Phys., 17, 4229–4249, https://doi.org/10.5194/acp-17-4229-2017, 2017.

Table 1. Summary of optical coefficients and chemical species in Xi'an observed in the entire campaign, normal period 695 (January 1st to 23rd, 2020~~1 to 23 January~~), and COVID-19 lockdown period (January 27th to February 7th, 2020~~27 January to 7 February~~).

Parameters[*]	Entire campaign	Normal period	COVID-19 lockdown period	Change ratio[**]
Optical coefficients				
b_{scat}	623.2 ±248.3	688.1 ±261.4	498.4 ±159.0	27.6%
b_{abs}	72.6 ±42.1	86.6 ±43.0	45.9 ±22.9	47.0%
b_{ext}	695.8 ±285.3	774.7 ±298.1	544.3 ±179.4	29.7%
SSA	0.90 ±0.03	0.89 ±0.03	0.92 ±0.02	-3.2%
Chemical species				
$PM_{2.5}$	116.4 ±56.3	134.4 ±56.9	81.8 ±34.9	39.1%
NH_4NO_3	33.1 ±17.3	40.2 ±16.4	19.5 ±8.8	51.6%
$(NH4)_2SO_4$	8.3 ±4.6	9.5 ±4.9	5.9 ±2.5	38.1%
fine soil	11.8 ±8.0	15.8 ±7.2	4.3 ±1.9	72.5%
BC	4.4 ±2.6	5.4 ±2.6	2.7 ±1.3	50.6%
POA	18.3 ±12.4	20.9 ±12.7	13.4 ±10.1	35.8%
LO-OOA	7.6 ±5.8	8.6 ±6.4	5.6 ±3.7	34.7%
MO-OOA	11.1 ±4.5	12.0 ±4.8	9.5 ±3.3	20.9%

[*]The units for b_{scat}, b_{abs}, b_{ext} are Mm^{-1}; SSA is dimensionless; The units of chemical species are μg m^{-3}.

[**]Change ratio = ([Normal period] − [COVID-19 lockdown period])/[Normal period]×100%.

700 **Table 2.** Estimated MSEs and MAEs (m^2 g^{-1}) of individual chemical components during normal and COVID-19 lockdown periods.

Components	Normal period		COVID-19 lockdown period	
	MSE	MAE	MSE	MAE
NH_4NO_3	3.74 ±0.18		3.23 ±0.18	
$(NH_4)_2SO_4$	7.35 ±0.25		4.78 ±0.35	
fine soil	2.46 ±0.35		3.39 ±0.79	
BC		15.00		13.27
POA	3.90 ±0.18	0.25 ±0.01	3.48 ±0.16	0.29 ±0.01
LO-OOA	8.62 ±0.27	0.27 ±0.02	9.87 ±0.35	0.59 ±0.03
MO-OOA	9.87 ±0.45	/	12.89 ±0.55	0.31 ±0.04

[*]MAE of MO-OOA during the normal period was negative (near zero) and not listed in the table.
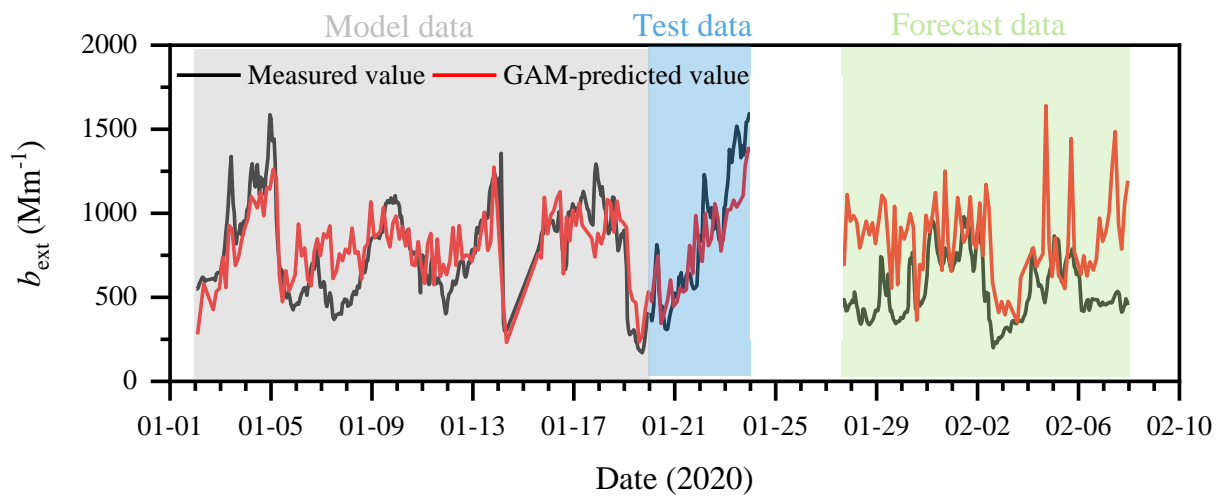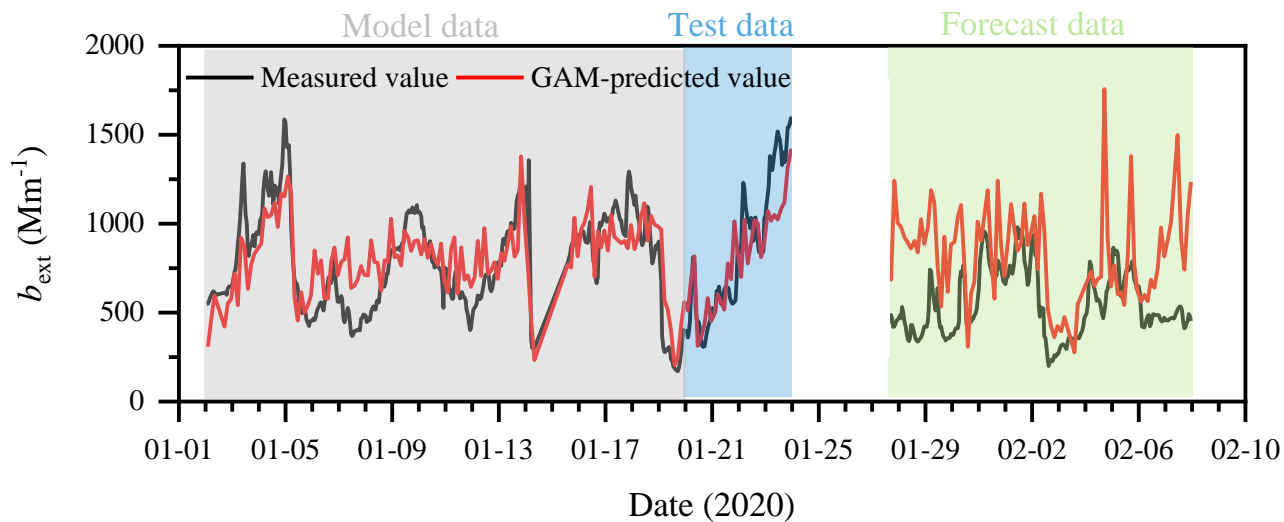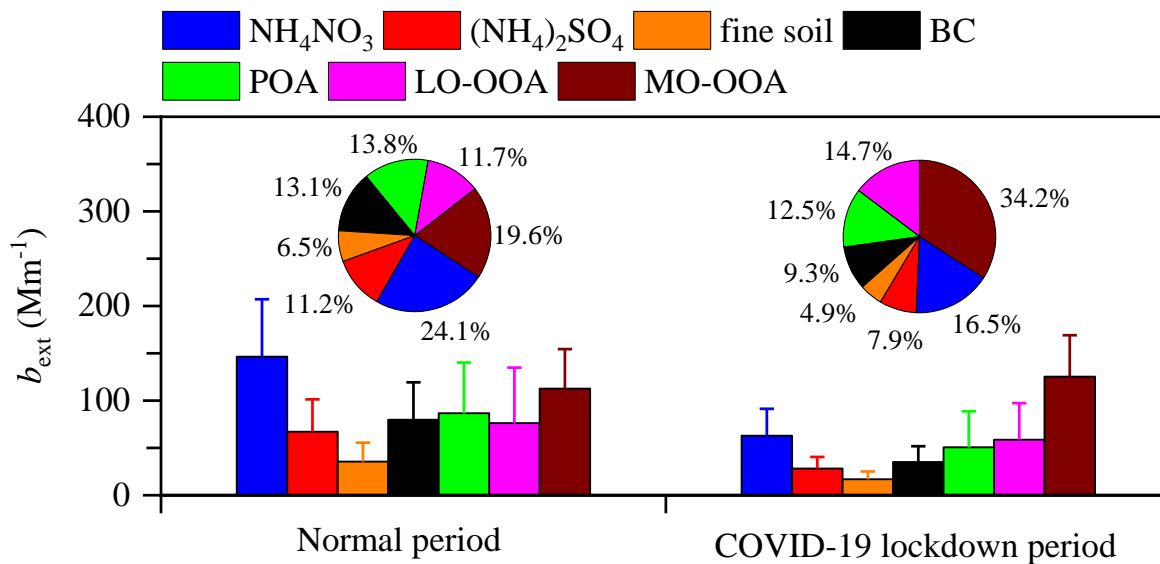
Figure captions:

Figure 1. Hourly variations of light scattering (b_{scat}), absorption (b_{abs}), and extinction (b_{ext}) coefficients, single scattering albedo (SSA), and PM$_{2.5}$ mass concentrations in Xi'an during the normal (January 1st to 23rd, 2020~~1 to 23 January~~) and COVID-19 lockdown (January 27th to February 7th, 2020~~27 January to 7 February~~) periods.

Figure 2. Variations of single scattering albedo (SSA) as a function of (a) secondary inorganic aerosol (SIA = NH$_4$NO$_3$ + (NH$_4$)$_2$SO$_4$)/PM$_{2.5}$, (b) secondary organic aerosol (SOA = LO-OOA + MO-OOA)/OA, and (c) LO-OOA/MO-OOA ratios during the normal and COVID-19 lockdown periods.

Figure ~~1~~3. Time series of the measured and GAM-predicted light extinction coefficient (b_{ext}) for the model data, test data, and forecast data.

Figure ~~2~~4. Contributions of NH$_4$NO$_3$, (NH$_4$)$_2$SO$_4$, fine soil, BC, POA, LO-OOA, and MO-OOA to the reconstructed chemical light extinction coefficient (b_{ext}) during the normal and COVID-19 lockdown periods.
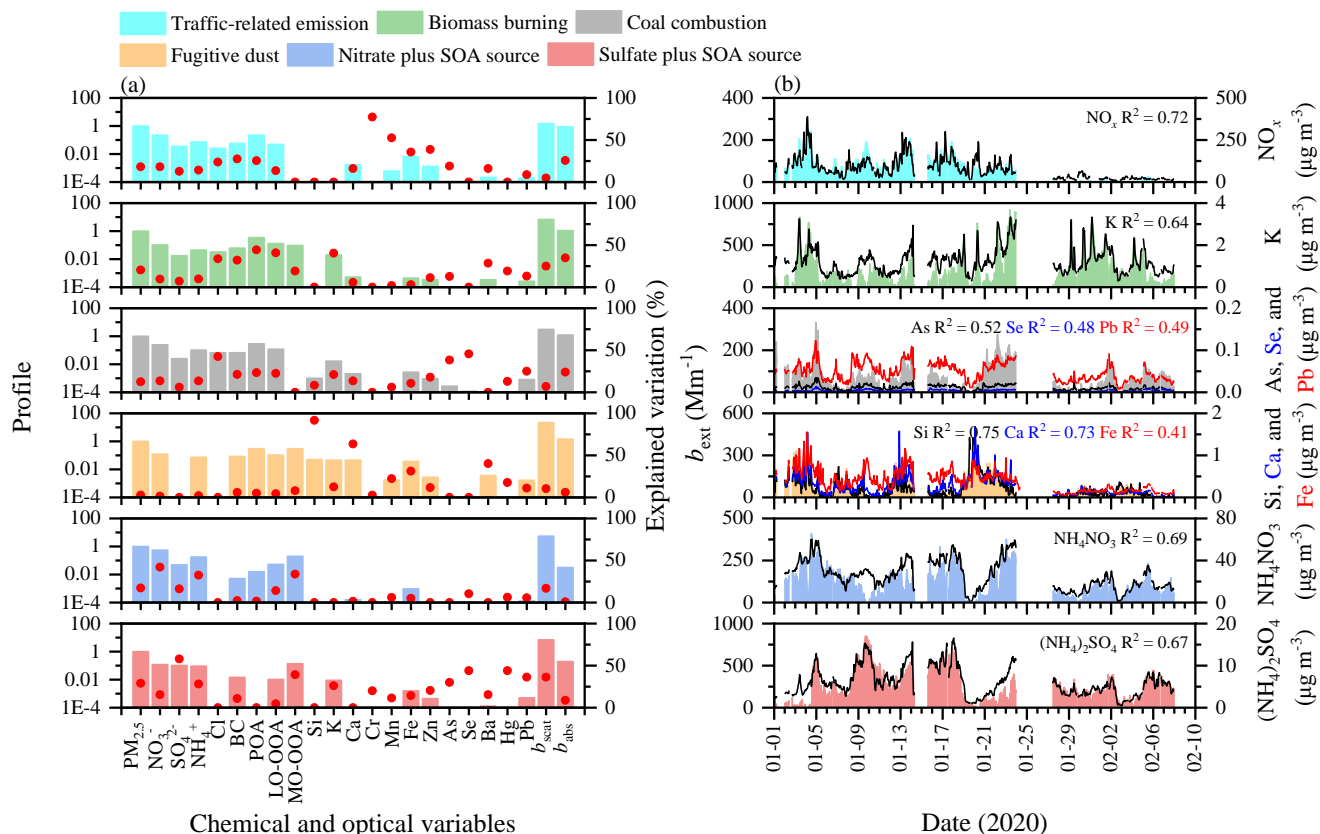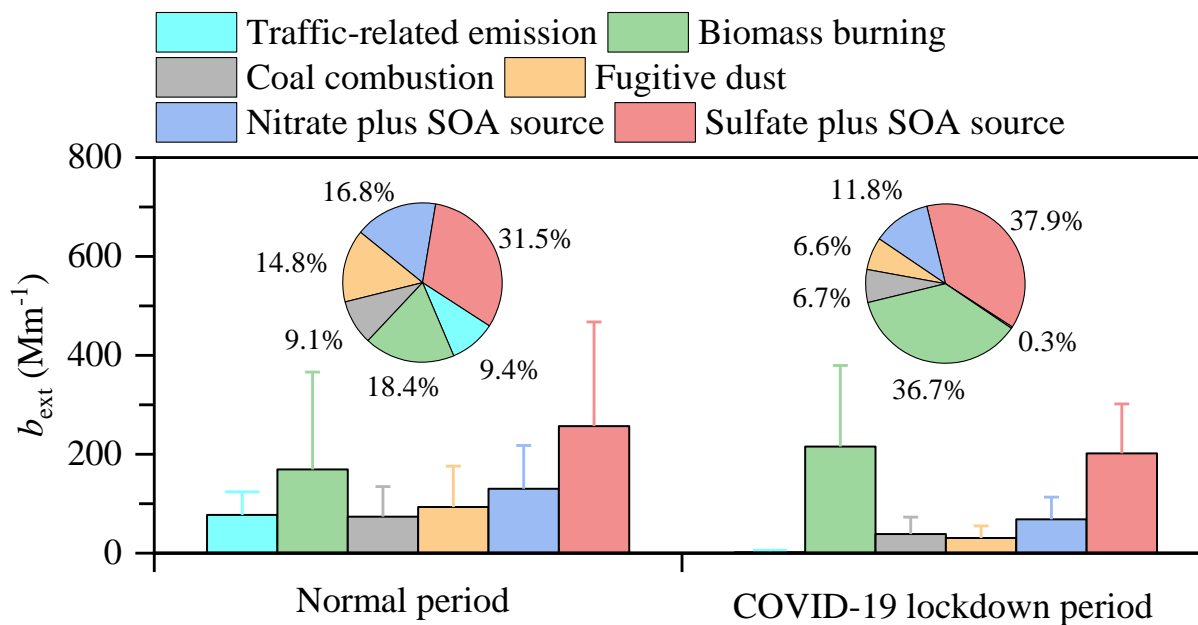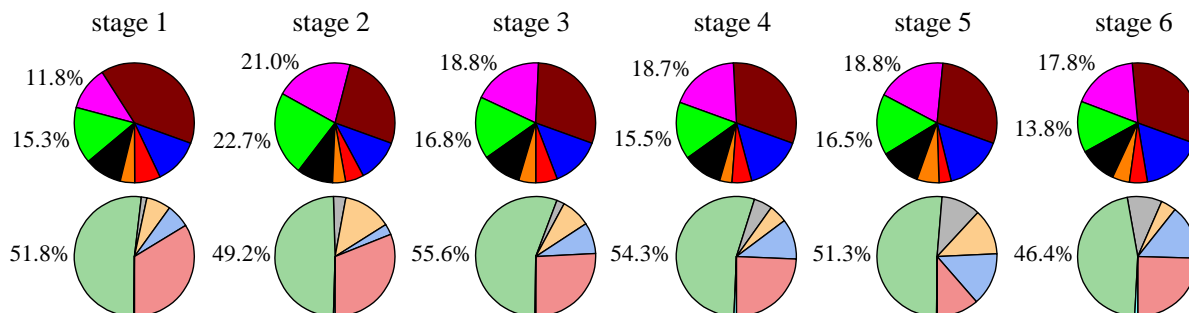
Figure ~~3~~5. (a) Profiles and (b) time series plots of the resolved source factors in the six~~6~~-factor solution, including traffic-related emission, biomass burning, coal combustion, fugitive dust, nitrate plus SOA source, and sulfate plus SOA source. The columns in each factor are~~is~~ the profile that display~~sing~~ the relative relation of absolute values of variables. The red dot represents the explained variation of species for different factors. The corresponding time trends of chemical tracers are also shown.

Figure ~~4~~6. Contributions of six resolved sources to the modeled source light extinction coefficient (b_{ext}) 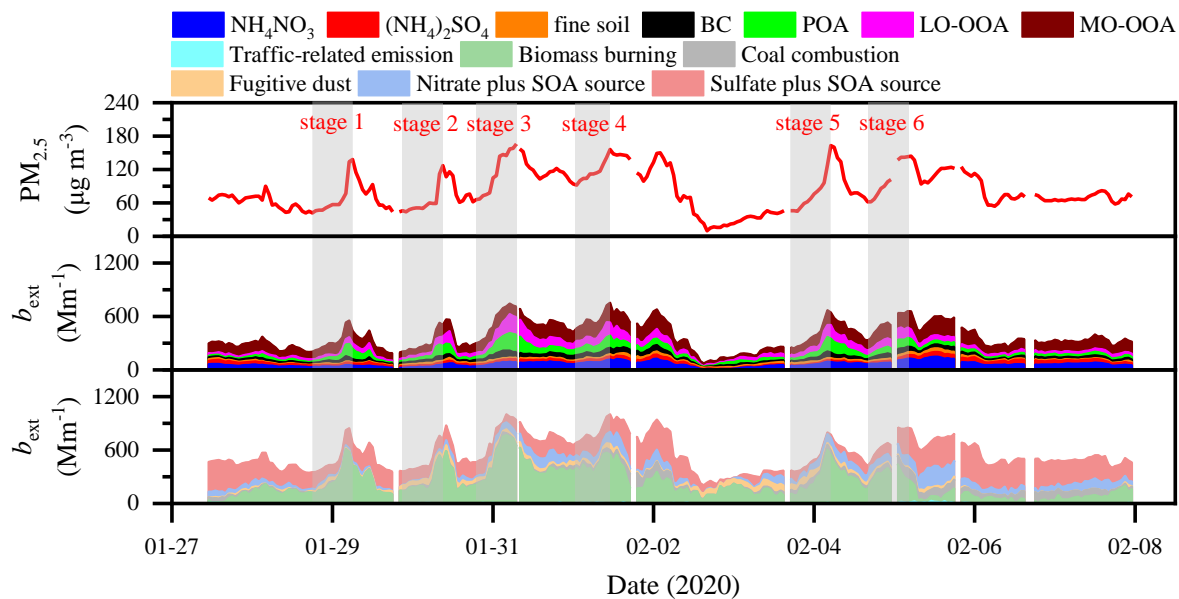during the normal and COVID-19 lockdown periods, including traffic-related emission, biomass burning, coal combustion, fugitive dust, nitrate plus SOA source, and sulfate plus SOA source.
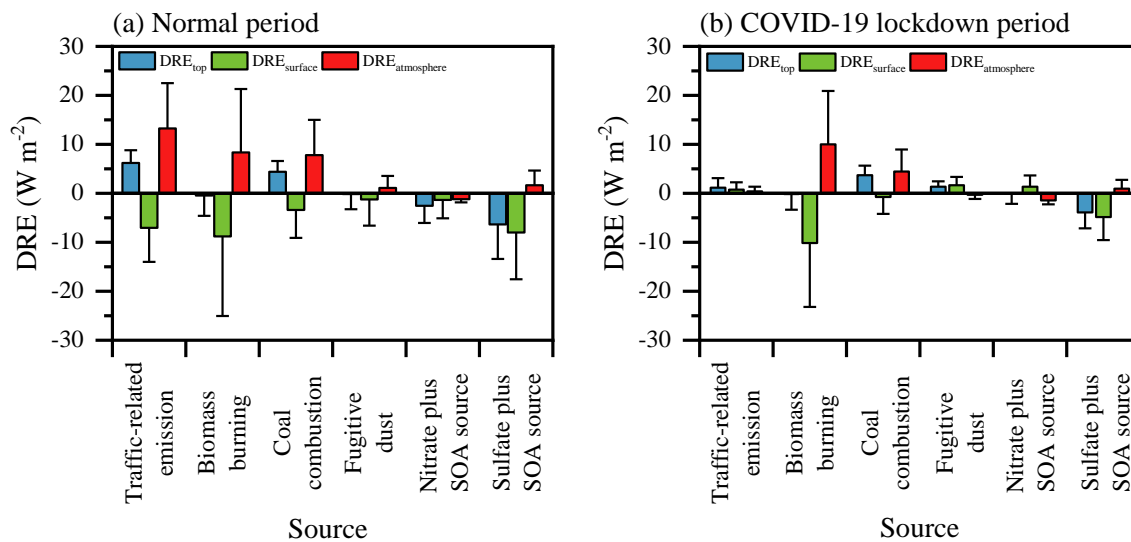
Figure ~~5~~7. Time series of PM$_{2.5}$ mass concentration, the light extinction coefficient (b_{ext}) of chemical species, and the b_{ext} from six resolved sources during the lockdown period. Pie charts depicting the average fractional contributions of chemical species and sources to b_{ext} during the PM$_{2.5}$ rising stages, which were marked in light gray.

Figure ~~6~~8. Direct radiative effect (DRE) of aerosol from traffic-related emission, biomass burning, coal combustion, fugitive dust, nitrate plus SOA source, and sulfate plus SOA source at the earth's surface, the top of the atmosphere, and in the atmosphere during the normal (a) and COVID-19 lockdown (b) periods.

24

Figure 1. Hourly variations of light scattering (b_{scat}), absorption (b_{abs}), and extinction (b_{ext}) coefficients, single scattering albedo (SSA), and PM$_{2.5}$ mass concentrations in Xi'an during the normal (January 1st to 23rd, 2020~~1 to 23 January~~) and COVID-19 lockdown (January 27th to February 7th, 2020~~27 January to 7 February~~) periods.

25

Figure 2. Variations of single scattering albedo (SSA) as a function of (a) secondary inorganic aerosol (SIA = NH_4NO_3 + $(NH_4)_2SO_4$)/$PM_{2.5}$, (b) secondary organic aerosol (SOA = LO-OOA + MO-OOA)/OA, and (c) LO-OOA/MO-OOA ratios during the normal and COVID-19 lockdown periods.

740   **Figure 1̶3.** Time series of the measured and GAM-predicted light extinction coefficient (b_{ext}) for the model data, test data, and forecast data.

Figure 24. Contributions of NH_4NO_3, $(NH_4)_2SO_4$, fine soil, BC, POA, LO-OOA, and MO-OOA to the reconstructed
745 chemical light extinction coefficient (b_{ext}) during the normal and COVID-19 lockdown periods.

Figure 35. (a) Profiles and (b) time series plots of the resolved source factors in the six6-factor solution, including traffic-related emission, biomass burning, coal combustion, fugitive dust, nitrate plus SOA source, and sulfate plus SOA source. The columns in each factor areis the profile that displaysing the relative relation of absolute values of variables. The red dot represents the explained variation of species for different factors. The corresponding time trends of chemical tracers are also shown.

29

755 **Figure 46.** Contributions of six resolved sources to the modeled source light extinction coefficient (b_{ext}) during the normal and COVID-19 lockdown periods, including traffic-related emission, biomass burning, coal combustion, fugitive dust, nitrate plus SOA source, and sulfate plus SOA source.

Figure 57. Time series of PM$_{2.5}$ mass concentration, the light extinction coefficient (b_{ext}) of chemical species, and the b_{ext} from six resolved sources during the lockdown period. Pie charts depicting the average fractional contributions of chemical species and sources to b_{ext} during the PM$_{2.5}$ rising stages, which were marked in light gray.

Figure 68. Direct radiative effect (DRE) of aerosol from traffic-related emission, biomass burning, coal combustion, fugitive dust, nitrate plus SOA source, and sulfate plus SOA source at the earth's surface, the top of the atmosphere, and in the atmosphere during the normal (a) and COVID-19 lockdown (b) periods.

Supplement of

Measurement report: The importance of biomass burning in light extinction and direct radiative effect of urban aerosol during the COVID-19 lockdown in Xi'an, China

Jie Tian[1,2], Qiyuan Wang[1,2,3], Huikun Liu[1], Yongyong Ma[4], Suixin Liu[1,2], Yong Zhang[1], Weikang Ran[1], Yongming Han[1,2,3], and Junji Cao[5]

[1]State Key Laboratory of Loess and Quaternary Geology, Institute of Earth Environment, Chinese Academy of Sciences, Xi'an 710061, China
[2]CAS Center for Excellence in Quaternary Science and Global Change, Xi'an 710061, China
[3]~~Guanzhong Plain Ecological Environment Change and Comprehensive Treatment~~ National Observation and Research Station of Regional Ecological Environment Change and Comprehensive Management in the Guanzhong Plain, Shaanxi, Xi'an 710061, China
[4]Meteorological Institute of Shaanxi Province, Xi'an 710015, China
[5]Institute of Atmospheric Physics, Chinese Academy of Sciences, Beijing 100029, China

Correspondence: Qiyuan Wang (wangqy@ieecas.cn) and Junji Cao (jjcao@mail.iap.ac.cn)

17   **Text S1.** Absorption Ångström exponent method

18   In this study, aerosol light absorption coefficient (b_{abs}) at wavelengths of λ = 370 nm, 470 nm, 520 nm,

19   590 nm, 660 nm, and 880 nm were measured by a newly developed Aethalometer (model AE33, Magee

20   Scientific, Berkeley, CA, USA). The Absorption Ångström exponent (AAE) describes the wavelength

21   dependence of aerosol light absorption, and can be calculated according to power law fitting ~~of~~ b_{abs}

22   at~~from~~ wavelengths of 370 nm to 880 nm (Moosmüller et al., 2011) as below:

23                                      $$b_{abs}(\lambda) \sim \lambda^{-AAE}$$ (1)

24   Through the AAE method (Lack and Langridge, 2013), the mass absorption efficiency (MAE) of black

25   carbon (BC) at 520 nm can be obtained as follows:

26                          $$b_{abs}(520 \text{ nm}) = b_{abs\text{-}BC}(520 \text{ nm}) + b_{abs\text{-}BrC}(520 \text{ nm})$$ (2)

27                          $$b_{abs\text{-}BC}(520 \text{ nm}) = b_{abs\text{-}BC}(880 \text{ nm}) \times \left(\frac{520}{880}\right)^{-AAE_{BC}}$$ (3)

28                          $$MAE_{BC}(520 \text{ nm}) = \frac{b_{abs\text{-}BC}(520 \text{ nm})}{[BC]}$$ (4)

29   where b_{abs}-BC and b_{abs}-BrC in Mm^{-1} are the light absorption coefficients caused by BC and brown

30   carbon (BrC), respectively; AAE_{BC} is the AAE caused by the BC particle, which can vary from 0.8 to

31   1.4 due to core size, coating materials, and mixing state (Lack and Cappa, 2010; Lack and Langridge,

32   2013). The linear relationship between the AAEs and the mass concentration ratios of organic aerosol

33   (OA) to BC is investigated to find the realistic AAE_{BC} during the normal and lockdown periods (Figure

34   ~~S13~~S12) (Yuan et al., 2016); and [BC] is the mass concentration of BC in μg m^{-3}.

45   **Text S2.** U~~The u~~ncertainty of the element <u>concentration</u>

46   Considering the element concentration measured by the Xact 625 ambient metals monitor with <u>a</u> 1-<u>-</u>hour

47   sampling interval, the uncertainty of the element <u>concentration</u> (u_e) inputting into the receptor model

48   was estimated as follows (Norris et al., 2014):

49    $$u_e = \sqrt{(c_e \times 10\%)^2 + (0.5 \times MDL)^2}, \text{ for } c_e > MDL \tag{5}$$

50    $$u_e = \frac{5}{6} \times MDL, \text{ for } c_e \leq MDL \tag{6}$$

51   where c_e is the concentration of the element; 10% is the default analytical relative error (Rai et al., 2020);

52   <u>and</u> MDL represents <u>the</u> method detection limit <u>of</u> ~~for~~ the element.

53 **Text S3.** Diagnostics of HERM solutions

54 In this study, factor numbers from two2 to eight8 were selected to run in the HERM software. Each

55 factor solution was performed with completely unconstrained profiles at twenty different seeds to

56 explore the possible sources. Detailed information on how the most interpretable factors were selected

57 is presented below.

58 As shown in Figure S2, the values of Q/Q_{exp} (> 1) decreased as the factor numbers increased. The large

59 Q/Q_{exp} values in two2- (21.10 ±0.03) and three3-factor (12.29 ±0.01) solutions indicated too few factors

60 were resolved. In the four4-factor solution (Figure S3), Factor 2 identified as biomass burning was

61 characterized by high explained variations (EV) values of POA (56%), LO-OOA (54%), BC (43%), Cl

62 (55%). Factor 3 was regarded as fugitive dust due to significant EV values of Si (100%), Ca (68%), and

63 Fe (35%). For the Factor 4 assigned to the secondary source, EV values of NO_3^-, SO_4^{2-}, NH_4^+, and MO-

64 OOA were larger than 30%. It is noted that Factor 1 was associated with the traffic-like source because

65 b_{ext} from this source showed a moderate correlation with NO_x, a tracer of fresh motor vehicle exhaust

66 emission ($R^2 = 0.58$). However, the high EV values of some specific elements (e.g., As (44%) and Se

67 (31%)) in this factor indicated the possible mixture of other fossil fuel sources (e.g., coal combustion).

68 When five factors were resolved, except traffic-like source (Factor 1), biomass burning (Factor 2), and

69 fugitive dust (Factor 3), the secondary source was split into nitrate plus SOA (Factor 4) and sulfate plus

70 SOA (Factor 5) sources (Figure S4). The increase to six6-factor solution (Figure S5) showed well

71 separation of traffic-related emission (Factor 1) and coal combustion (Factor 3). The A stronger

72 correlation between b_{ext} from traffic-related emission and NO_x ($R^2 = 0.72$) was found compared to

73 traffic-like factors resolved in four4— and five5- factor solutions ($R^2 = 0.58$). As shown in Figures S6

74 and S7, further investigations of unconstrained profile solutions with seven7 and —eight8 factors resulted

75 in factor split. The extra split factors possibly came from biomass burning and coal combustion, mainly

76 due to high EV values of K (26%–33%), or As (21%). Despite b_{ext} from coal combustion factors in

77 seven7- and eight8- factor solutions showed the stronger correlation with As ($R^2 = 0.63$–0.68), Se (R^2

78 = 0.79–0.86), and Pb ($R^2 = 0.60$–0.67), the profiles identified coal combustion had no POA contribution.

79 Meanwhile, the values of POA in fugitive dust profiles identified in seven7— and eight8- factor solutions

80 were higher than 1 (the reference standard of $PM_{2.5}$). It is indicated that these profiles did no2t match the
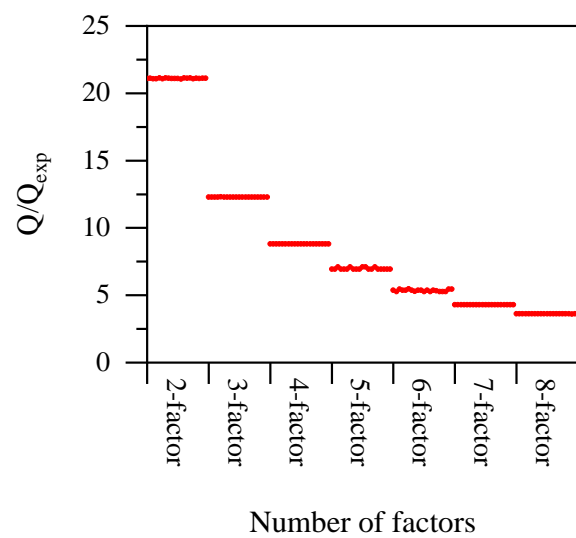
81 real world.

82 Therefore, for our analyses of all as the factor solutions described above, six factors were the most

83 interpretable in our study, including traffic-related emission, biomass burning, coal combustion, fugitive

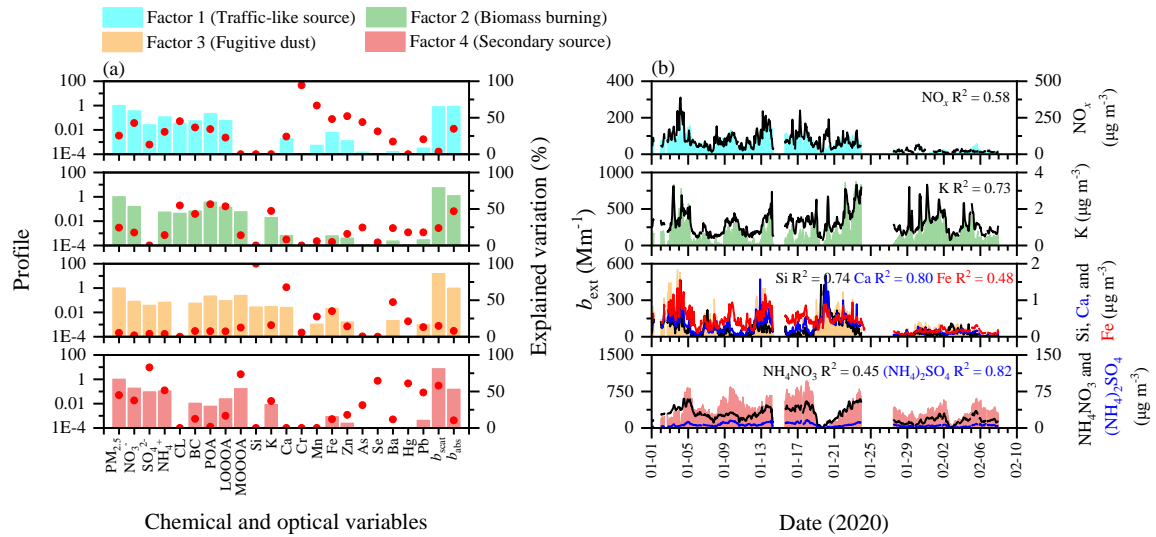84 dust, nitrate plus SOA source, and sulfate plus SOA source.
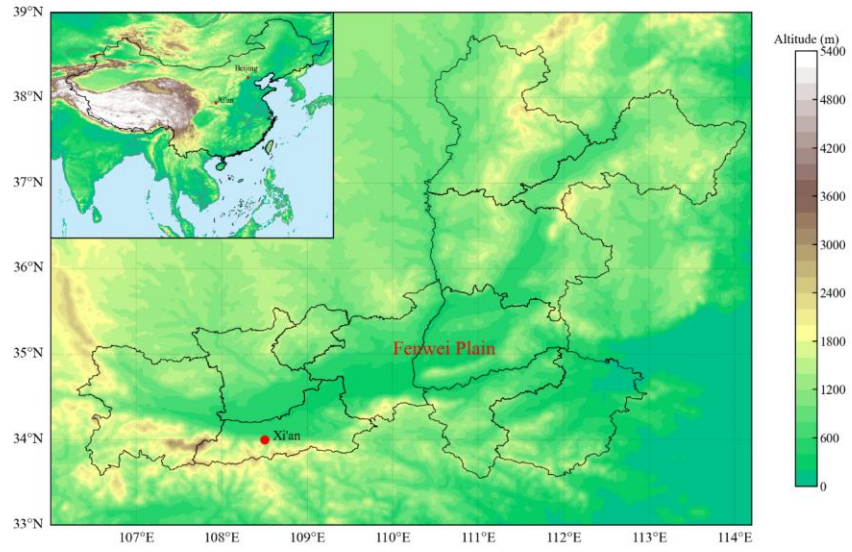
85

86   **Figure S1.** The location of <u>the</u> sampling site in Xi'an, China.

87

88 **Figure S2.** Values of Q/Q_{exp} for the unconstrained profile solutions with two2 to eight 8 factors at
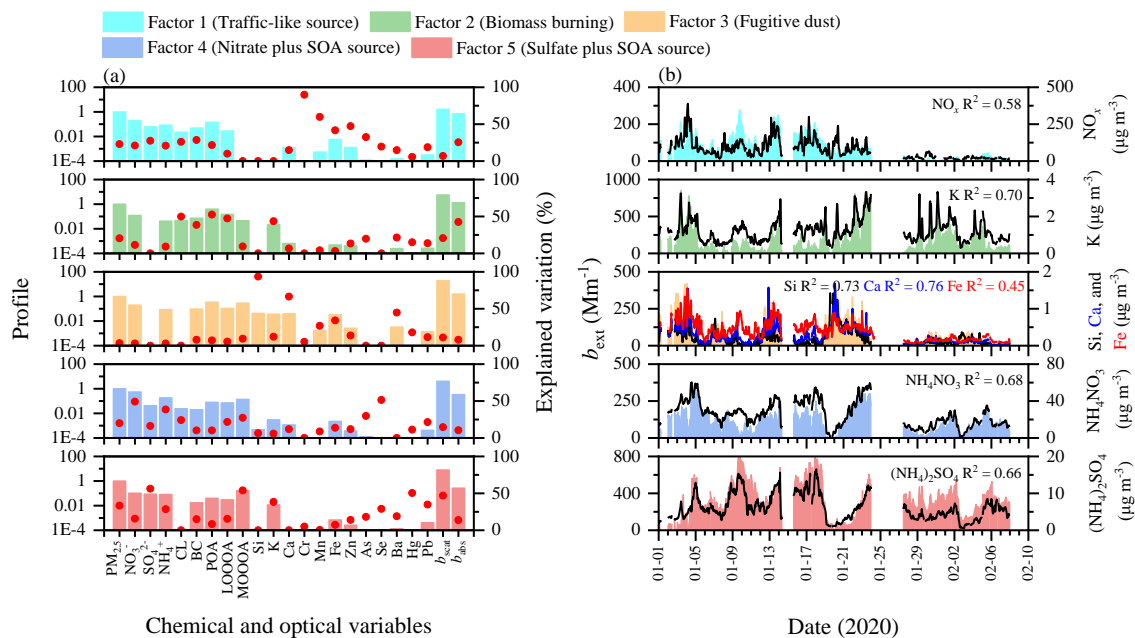89 twenty different seeds.
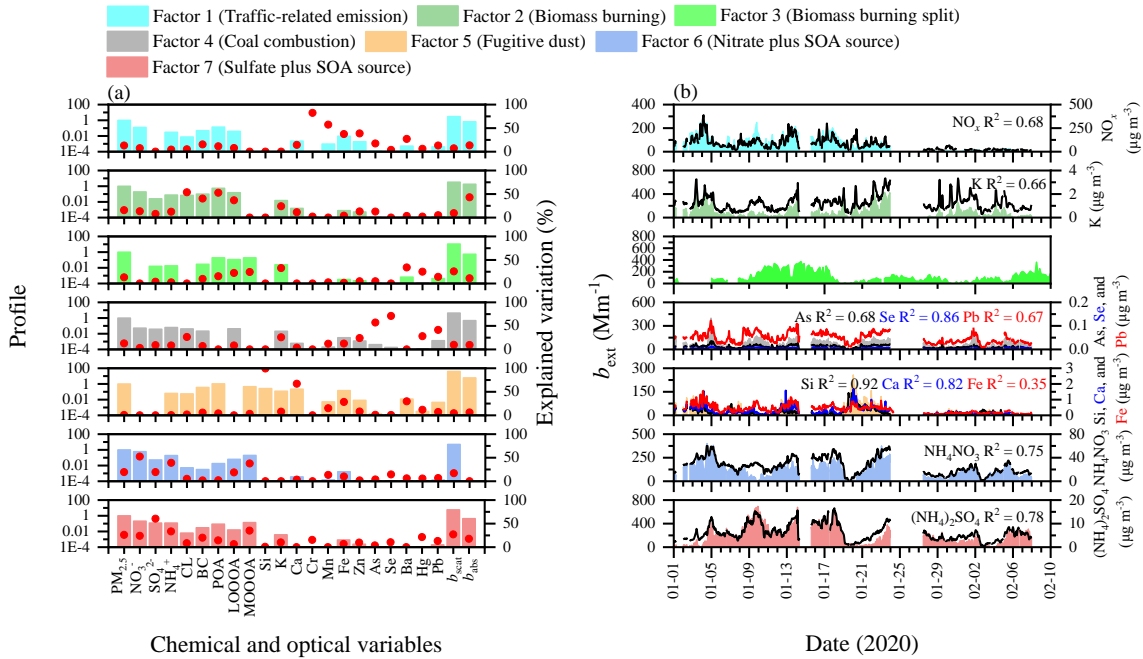
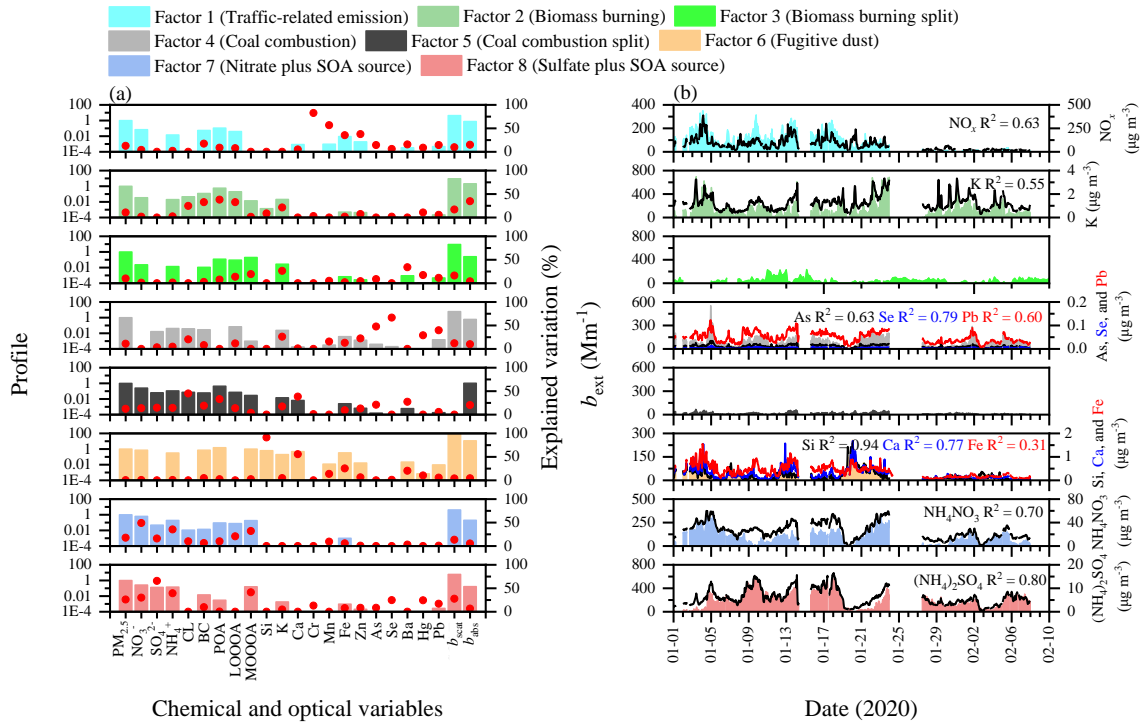**Figure S3.** (a) Profiles and (b) time series plots of the resolved source factors in the ~~four~~4-factor solution. The columns in each factor ~~are~~is the profile that ~~display~~sing ~~the~~ relative relation of absolute values of variables. The red dot represents the explained variation of species for different factors. The corresponding time trends of chemical tracers also are shown.

Figure S4. (a) Profiles and (b) time series plots of the resolved source factors in the five5-factor solution. The columns in each factor areis the profile that displaysing the relative relation of absolute values of variables. The red dot represents the explained variation of species for different factors. The corresponding time trends of chemical tracers also are shown.
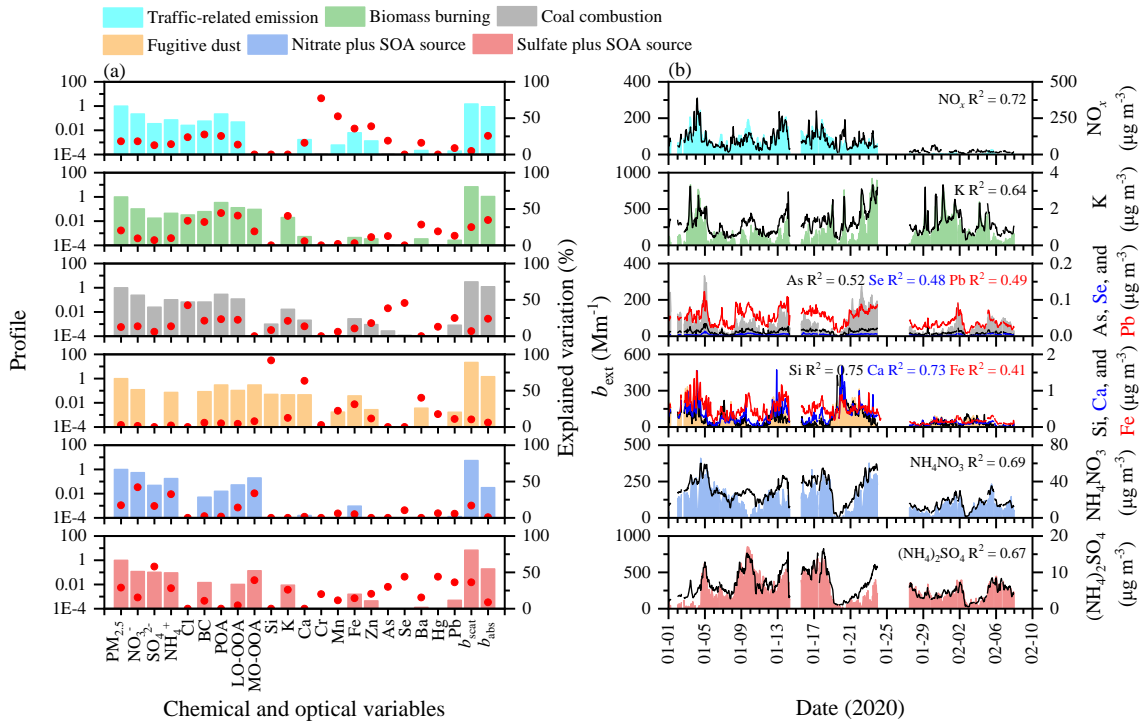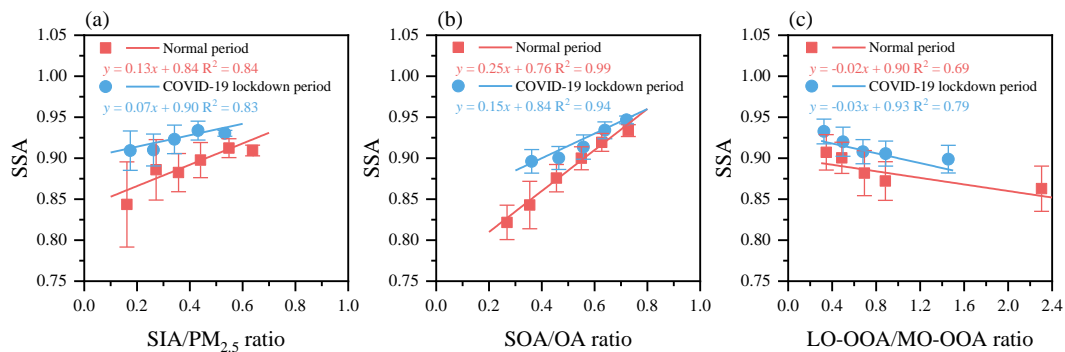
Figure S5. (a) Profiles and (b) time series plots of the resolved source factors in the six6-factor solution. The columns in each factor areis the profile that displays theing relative relation of absolute values of variables. The red dot represents the explained variation of species for different factors. The corresponding time trends of chemical tracers also are shown.

Figure S6. (a) Profiles and (b) time series plots of the resolved source factors in the seven7-factor solution. The columns in each factor areis the profile that displays theing relative relation of absolute values of variables. The red dot represents the explained variation of species for different factors. The corresponding time trends of chemical tracers also are shown.

Figure S7. (a) Profiles and (b) time series plots of the resolved source factors in the eight8-factor
solution. The columns in each factor areis the profile that displays theing relative relation of absolute
values of variables. The red dot represents the explained variation of species for different factors. The
corresponding time trends of chemical tracers also are shown.
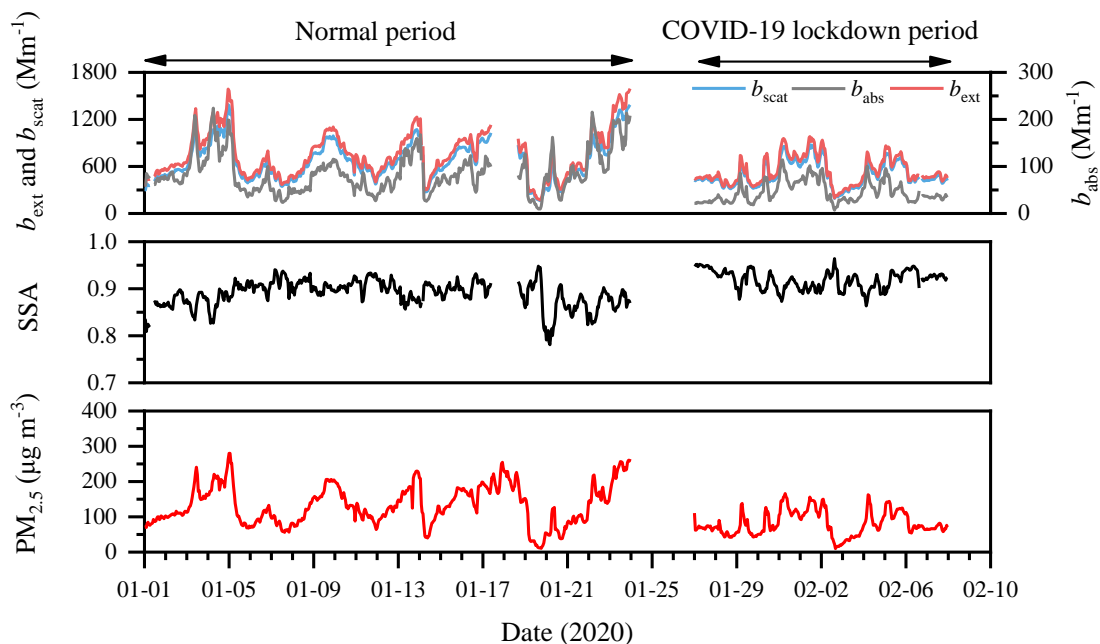
Figure S8. Hourly variations of light scattering (b_{scat}), absorption (b_{abs}), and extinction (b_{ext}) coefficients, single scattering albedo (SSA), and $PM_{2.5}$ mass concentrations in Xi'an during the normal (1 to 23 January) and COVID-19 lockdown (27 January to 7 February) periods.

(a)
y = 0.13x + 0.84 R² = 0.84
y = 0.07x + 0.90 R² = 0.83

(b)
y = 0.25x + 0.76 R² = 0.99
y = 0.15x + 0.84 R² = 0.94

(c)
y = -0.02x + 0.90 R² = 0.69
y = -0.03x + 0.93 R² = 0.79

Figure S9. Variations of single scattering albedo (SSA) as a function of (a) secondary inorganic aerosol (SIA = NH_4NO_3 + $(NH_4)_2SO_4$)/$PM_{2.5}$, (b) secondary organic aerosol (SOA = LO-OOA + MO-OOA)/OA, and (c) LO-OOA/MO-OOA ratios during the normal and COVID-19 lockdown periods.
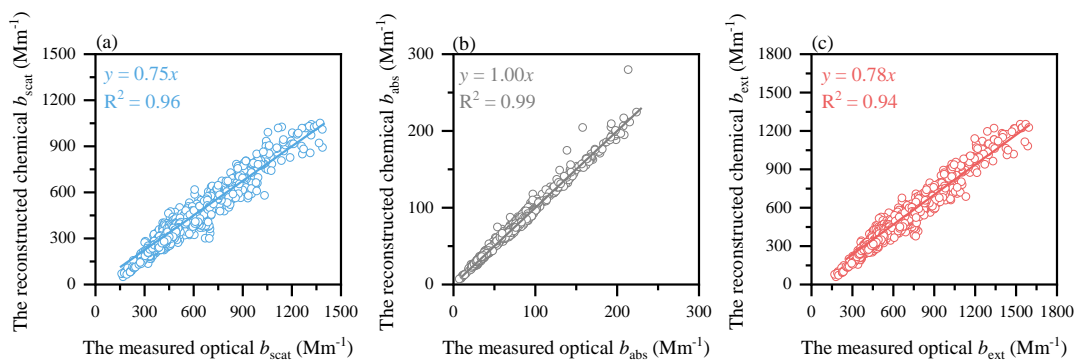
123

124   **Figure S8~~10~~.** Linear relationships between the reconstructed chemical and the measured optical (a) b_{scat},
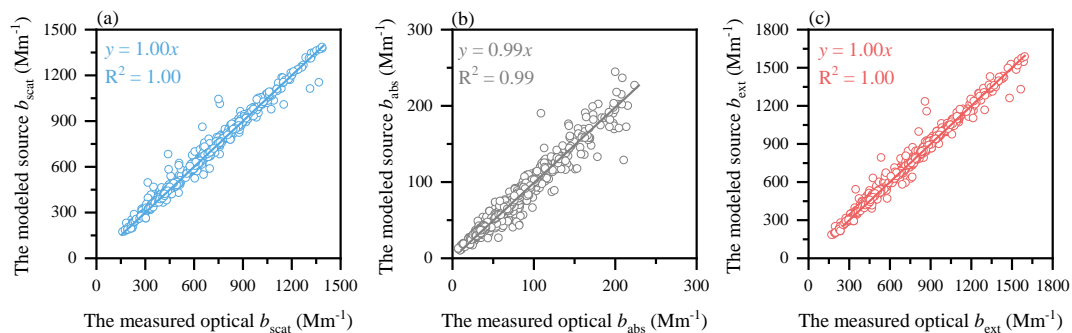
125   (b) b_{abs}, and (c) b_{ext}.
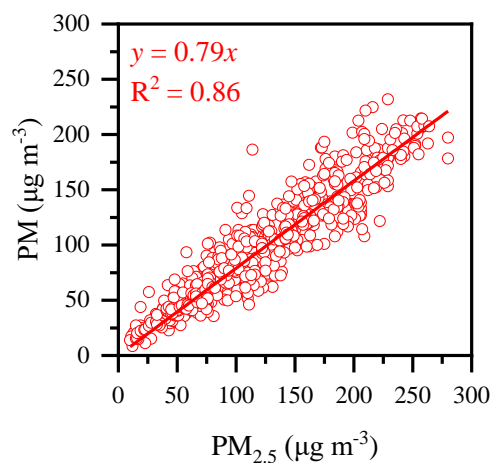
Figure S911. Linear relationships between PM$_{2.5}$ and PM used in the reconstruction of aerosol optical coefficients. PM is the sum of NH$_4$NO$_3$, (NH$_4$)$_2$SO$_4$, fine soil, BC, POA, LO-OOA, and MO-OOA in this study. The slope of the linear regression between PM$_{2.5}$ and PM concentrations (0.79) was close to that between the measured optical b_{ext} and the reconstructed chemical b_{ext} (0.78, see Figure S810c), suggesting that chemical calculation of b_{ext} was a reasonable estimation of aerosol optical coefficients by using chemical components data.
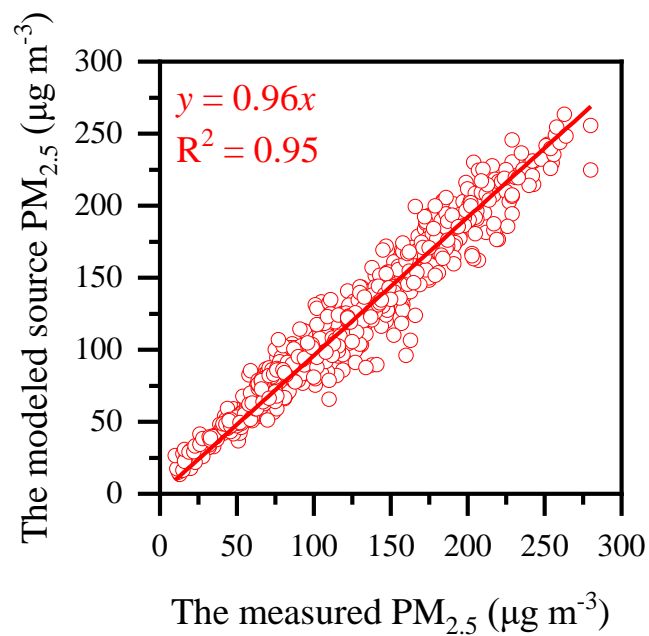
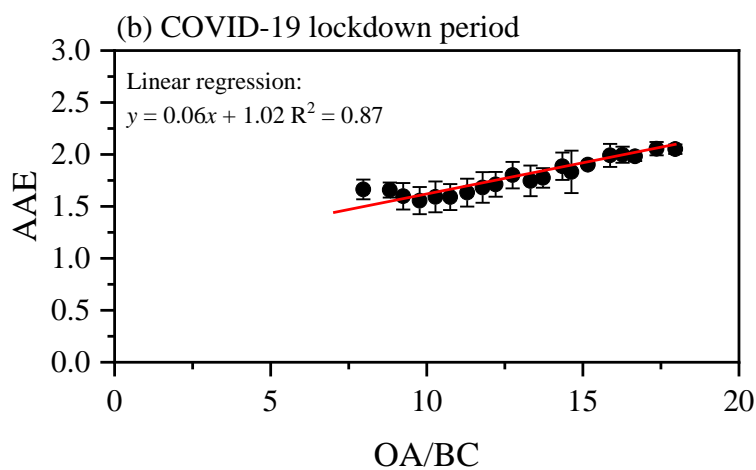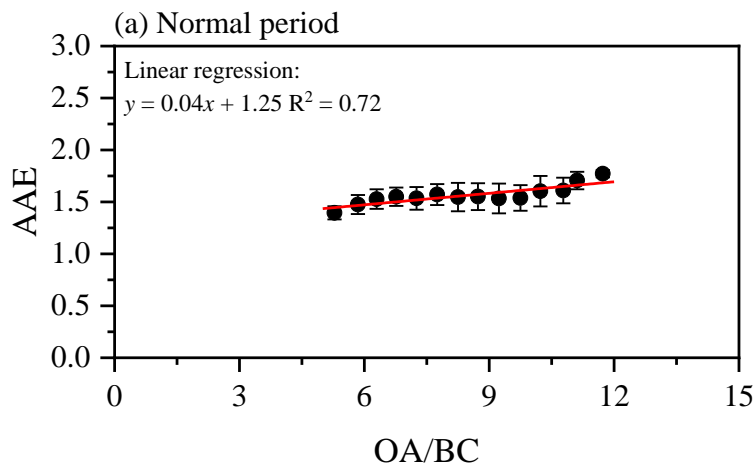**Figure S10.** Linear relationship between the modeled source and the measured $PM_{2.5}$ mass concentration. The modeled source $PM_{2.5}$ was strongly correlated linearly with the measured optical $PM_{2.5}$ ($R^2 = 0.95$, slope = 0.96), indicating that the six identified sources can adequately account for the variability in $PM_{2.5}$ mass concentration.
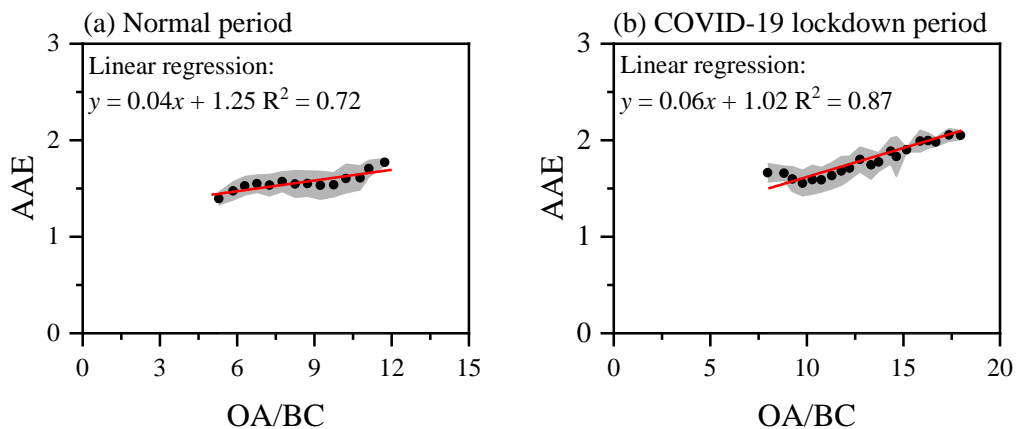
139

Figure S11̶2̶. Linear relationships between the modeled source and the measured optical (a) b_{scat}, (b) b_{abs}, and (c) b_{ext}. The modeled source b_{scat}, b_{abs}, and b_{ext} were̶a̶s̶ strongly correlated linearly with the measured optical b_{scat} (R^2 = 1.00, slope = 1.00), b_{abs} (R^2 = 0.99, slope = 0.99), and b_{ext} (R^2 = 1.00, slope = 1.00), indicating that the six identified sources can adequately account for the variability in aerosol optical coefficientsb_{ext}.

(a) Normal period

Linear regression:
$y = 0.04x + 1.25$ $R^2 = 0.72$

(b) COVID-19 lockdown period

Linear regression:
$y = 0.06x + 1.02$ $R^2 = 0.87$

(a) Normal period

Linear regression:
$y = 0.04x + 1.25$ $R^2 = 0.72$

(b) COVID-19 lockdown period

Linear regression:
$y = 0.06x + 1.02$ $R^2 = 0.87$

Figure S123. LThe linear relationships between the AAEs and the mass concentration ratios of organic aerosol (OA) to BC (OA/BC) during the normal (a) and lockdown (b) periods. The intercept of the linear regression represents the realistic AAE_{BC}. The points and light gray shadows represent the mean values and error margins in each bin ($\Delta(OA/BC) = 0.5$).

151 **Table S1.** Summary of chemical and meteorological measurements of in Xi'an before and during the

152 COVID-19 lockdown period.

Parameters	Sampling interval	Instruments and online source	Operation and calibration
Chemical variables			
NO_3^-, SO_4^{2-}, NH_4^+, Cl^-, and OA	15-min	Quadrupole aerosol chemical speciation monitor (Q-ACSM, Aerodyne Research Inc., Billerica, Massachusetts, USA)	The relative ionization efficiencies (RIEs) for OA, nitrate, and chloride were set to 1.4, 1.1, and 1.3 by default, respectively. The RIE for ammonium (5.8) was determined from the ammonium nitrate aerosol calibration, while the RIE for sulfate (1.9) was estimated by fitting the measured sulfate versus predicted sulfate values. The collection efficiency was set to 0.45.
Si, K, Ca, Cr, Mn, Fe, Zn, As, Se, Ba, Hg, and Pb	1-hour	Xact 625 ambient metals monitor (Xact 625i, Cooper Environmental Services, Beaverton, OR, USA)	Daily advanced quality assurance checks were performed during 30 min after midnight to monitor shifts in the calibration.
$PM_{2.5}$ and NO_x	5-min	The Department of Ecology and Environment of Shaanxi Province (http://sthjt.shaanxi.gov.cn, in Chinese)	
Meteorological variables[*]			
WS, WD, ~~RH~~, T, P, and DP	1-hour	Integrated automatic weather station (MAWS201, Vaisala, Helsinki, Finland)	
PBLH	3-hour	Global Data Assimilation System (ftp://arlftp.arlhq.noaa.gov/pub/archives/gdas1)	PBLH at the sampling site was obtained using linear interpolation method.

153 [*]WS, WD, ~~RH~~, T, P, DP, and PBLH represent wind speed, wind direction, ~~relative humidity,~~

154 temperature, pressure~~s~~, dew point, and planetary boundary layer height, respectively.

155   **Table S2.** Summary of output indices from the constructed b_{ext} GAM.

Intercept	6.64~~0~~	
Adjusted R^2	0.54~~69~~	
~~IOA~~	~~0.909~~	

Smoothed parameters[*]	F value	p value
f(WS)	3.402~~194~~	0.002331~~341~~
f(WD)	5.820~~6.145~~	0.000134~~6.81×10⁻⁵~~
~~f(RH)~~	~~3.005~~	~~0.03216~~
f(T)	2.707~~575~~	0.01280~~969~~
f(P)	3.209~~268~~	0.001757~~1~~
f(DP)	13.325~~4.257~~	$\leq 2.00\times10^{-16}$
f(PBLH)	3.656~~4.249~~	0.026822~~1188~~

156   [*]WS, WD, ~~RH,~~ T, P, DP, and PBLH represent wind speed, wind direction~~, relative humidity~~,

157   temperature, pressure~~s~~, dew point, and planetary boundary layer height, respectively.

158   **Table S3.** Concurvity indices between each independent smoothed parameter in the constructed GAM.

Smoothed parameters[*]	f(WS)	f(WD)	f(T)	f(P)	f(DP)	f(PBLH)
f(WS)	1.00	0.28	0.03	0.09	0.07	0.23
f(WD)	0.15	1.00	0.08	0.09	0.03	0.07
f(T)	0.06	0.07	1.00	0.11	0.25	0.22
f(P)	0.08	0.24	0.08	1.00	0.06	0.09
f(DP)	0.05	0.06	0.08	0.07	1.00	0.05
f(PBLH)	0.13	0.07	0.05	0.04	0.06	1.00

159

Smoothed parameters[*]	f(WS)	f(WD)	f(RH)	f(T)	f(P)	f(DP)	f(PBLH)
f(WS)	1.00	0.27	0.09	0.03	0.09	0.08	0.23
f(WD)	0.16	1.00	0.05	0.08	0.10	0.03	0.07
f(RH)	0.08	0.10	1.00	0.04	0.03	0.36	0.33
f(T)	0.08	0.07	0.14	1.00	0.12	0.23	0.22
f(P)	0.09	0.23	0.07	0.05	1.00	0.07	0.09
f(DP)	0.05	0.06	0.36	0.08	0.06	1.00	0.05
f(PBLH)	0.13	0.07	0.32	0.06	0.05	0.08	1.00

160   [*]WS, WD, RH, T, P, DP, and PBLH represent wind speed, wind direction, relative humidity,

161   temperature, pressures, dew point, and planetary boundary layer height, respectively.

References

Lack, D. A.~~, and~~& Cappa, C. D.: Impact of brown and clear carbon on light absorption enhancement, single scatter albedo and absorption wavelength dependence of black carbon, Atmos. Chem. Phys., 10, 4207–4220, https://doi.org/10.5194/acp-10-4207-2010, 2010.

Lack, D. A. and~~, &~~ Langridge, J. M.: On the attribution of black and brown carbon light absorption using the Ångström exponent, Atmos. Chem. Phys., 13, 10535–10543, https://doi.org/10.5194/acp-13-10535-2013, 2013.

Moosmüller, H., Chakrabarty, R. K., Ehlers, K. M., and Arnott, W. P.: Absorption Ångström coefficient, brown carbon, and aerosols: basic concepts, bulk matter, and spherical particles, Atmos. Chem. Phys., 11, 1217–1225, https://doi.org/10.5194/acp-11-1217-2011, 2011.

Norris, G., Duvall, R., Brown, S., and Bai, S.: EPA positive matrix factorization (PMF) 5.0 fundamentals and user guide, 2014.

Rai, P., Furger, M., Slowik, J. G., Canonaco, F., Fröhlich, R., Hüglin, C., Minguillón, M. C., Petterson, K., Baltensperger, U., and Prévôt, A. S. H.: Source apportionment of highly time-resolved elements during a firework episode from a rural freeway site in Switzerland, Atmos. Chem. Phys., 20, 1657–1674, https://doi.org/10.5194/acp-20-1657-2020, 2020.

Yuan, J. F., Huang, X. F., Cao, L. M., Cui, J., Zhu, Q., Huang, C. N., Lan, Z .J., and He, L. Y.: Light absorption of brown carbon aerosol in the PRD region of China, Atmos. Chem. Phys., 16, 1433–1443, https://doi.org/10.5194/acp-16-1433-2016, 2016.